Science of the Total Environment 951 (2024) 175727

Contents lists available at ScienceDirect

Science of the Total Environment

journal homepage: www.elsevier.com/locate/scitotenv

Generation, characterization, and toxicological assessment of reference ultrafine soot particles with different organic content for inhalation toxicological studies

Anusmita Das [a,b], Jana Pantzke [a,b], Seongho Jeong [a,b], Elena Hartner [a,b], Elias J. Zimmermann [a,b], Nadine Gawlitta [a,*], Svenja Offer [a,b], Deeksha Shukla [a,b], Anja Huber [a,b], Narges Rastak [a], Arūnas Meščeriakovas [c], Natalia P. Ivleva [d], Evelyn Kuhn [a], Stephanie Binder [a,b], Thomas Gröger [a], Sebastian Oeder [a], Mathilde Delaval [a], Hendryk Czech [a,b], Olli Sippula [c,e], Jürgen Schnelle-Kreis [a], Sebastiano Di Bucchianico [a,b], Martin Sklorz [a,b], Ralf Zimmermann [a,b]

[a] Joint Mass Spectrometry Center (JMSC) at Comprehensive Molecular Analytics (CMA), Helmholtz Zentrum München, Ingolstädter Landstrasse 1, D-85764 Neuherberg, Germany
[b] Joint Mass Spectrometry Center (JMSC) at Chair of Analytical Chemistry, Institute of Chemistry, University of Rostock, Albert-Einstein-Strasse 27, D-18059 Rostock, Germany
[c] Department of Environmental and Biological Sciences, University of Eastern Finland, 70211 Kuopio, Finland
[d] Chair of Analytical Chemistry and Water Chemistry, Institute of Water Chemistry, TUM School of Natural Sciences, Department of Chemistry, Technical University of Munich, 85748 Garching, Germany
[e] Department of Chemistry, University of Eastern Finland, 80101 Joensuu, Finland

HIGHLIGHTS

- Two types of reference ultrafine soot particles (UFP) were produced
- Ultrafine soot UFP with similar physical properties and contrasting chemical properties
- The concentration of PAHs in the two types of UFP varied by orders of magnitude
- Different properties induce different toxicity *in vitro*
- Repeated UFP production and characterization proved excellent stability and repeatability

GRAPHICAL ABSTRACT

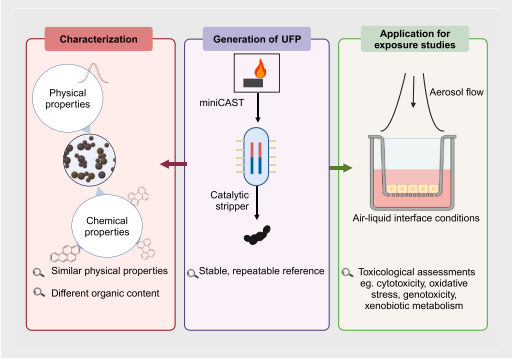

ARTICLE INFO

Editor: Hai Guo

ABSTRACT

Ultrafine particles (UFP) are the smallest atmospheric particulate matter linked to air pollution-related diseases. The extent to which UFP's physical and chemical properties contribute to its toxicity remains unclear. It is

* Corresponding author.
E-mail address: nadine.gawlitta@helmholtz-munich.de (N. Gawlitta).

https://doi.org/10.1016/j.scitotenv.2024.175727
Received 8 July 2024; Received in revised form 21 August 2024; Accepted 21 August 2024
Available online 22 August 2024

Keywords:
CAST
Soot
UFP
Black carbon
PAHs
Air-liquid interface exposure
In vitro toxicology

hypothesized that UFP act as carriers for chemicals that drive biological responses. This study explores robust methods for generating reference UFP to understand these mechanisms and perform toxicological tests.

Two types of combustion-related UFP with similar elemental carbon cores and physical properties but different organic loads were generated and characterized. Human alveolar epithelial cells were exposed to these UFP at the air-liquid interface, and several toxicological endpoints were measured. UFP were generated using a mini-CAST under fuel-rich conditions and immediately diluted to minimize agglomeration. A catalytic stripper and charcoal denuder removed volatile gases and semi-volatile particles from the surface. By adjusting the temperature of the catalytic stripper, UFP with high and low organic content was produced.

These reference particles exhibited fractal structures with high reproducibility and stability over a year, maintaining similar mass and number concentrations (100 $\mu g/m^3$, $2.0 \cdot 10^5$ $\#/cm^3$) and a mean particle diameter of about 40 nm. High organic content UFP had significant PAH levels, with benzo[*a*]pyrene at 0.2 % (m/m). Toxicological evaluations revealed that both UFP types similarly affected cytotoxicity and cell viability, regardless of organic load. Higher xenobiotic metabolism was noted for PAH-rich UFP, while reactive oxidation markers increased when semi-volatiles were stripped off. Both UFP types caused DNA strand breaks, but only the high organic content UFP induced DNA oxidation.

This methodology allows modification of UFP's chemical properties while maintaining comparable physical properties, linking these variations to biological responses.

1. Introduction

Ultrafine particles (UFP) are particulate matter (PM) which have an aerodynamic diameter of $\leq$0.1 μm. They are formed by the dynamic processes of nucleation of gas phase compounds followed by condensation and coagulation of primary particles (León-Mejía et al., 2016; Moreno-Ríos et al., 2022). They are produced by numerous natural sources like forest fires and volcanic events (Moreno-Ríos et al., 2022) while the anthropogenic sources include combustion sources like vehicular and power plant/ industrial emissions, biomass burning and tobacco smoking (Hofman et al., 2016; Schraufnagel, 2020). UFP have been investigated in multiple health-risk studies due to their small sizes (Leikauf et al., 2020; Ohlwein et al., 2019; Vallabani et al., 2023) which allows them to deposit with high efficiency down the alveolar regions of the respiratory system and further translocate throughout the body *via* the circulatory system (Han et al., 2023). Toxicological research indicates that UFP exhibit greater toxicity per unit of mass compared to larger particles, potentially playing a role in the onset and advancement of various diseases (Leikauf et al., 2020). In 2021, the World Health Organization (WHO) revised the recommendations for air quality, emphasizing UFP monitoring as a good practice statement and set stricter goal limits for PM $\leq$ 2.5 μm (Schwarz et al., 2023; WHO, 2021). However, epidemiological studies and experiment-based reference values for UFP are still lacking.

In vitro studies are valuable for investigating the cellular and molecular mechanisms of action of UFP. Air-Liquid Interface (ALI) exposure systems are becoming more and more common in respiratory toxicology for the direct deposition of aerosols deploying *in vitro* cells cultures (Singh et al., 2021; Upadhyay and Palmberg, 2018). The primary advantage of these systems lies in their operation that mimics more realistic exposure, where solid or liquid particles are often delivered in mixtures with the surrounding air and are directly deposited onto tissue-cell cultures (Paur et al., 2011; Thorne and Adamson, 2013). Current *in vitro* multi-well aerosol exposure systems facilitate exposure and assessment of aerosol in high performance systems with high capability, efficiency, and flexibility (Lucci et al., 2018). Using a computer model approach, Karg et al. (2020) demonstrated that aerosols with a size range of 40 to 450 nm, has comparable deposition in the ALI system to that in the lung regions. Many studies on UFP induced toxicity with ALI exposure methods use resuspension of collected filter samples (Diabaté et al., 2008; He et al., 2020) from combustion or ambient measurements. However, resuspension of collected UFP leads to substantial changes in morphology and chemical properties of the particles including losses of more volatile fractions (Roper et al., 2018, 2019). Other studies that investigated the toxicity of UFP at ALI exposure systems, such as studies on printer emissions (Kim et al., 2022), different fuel exhaust emissions (Hakkarainen et al., 2023; Mülhopt et al., 2016), aircraft cabin bleed air (He et al., 2021), aircraft turbine engines (Jonsdottir et al., 2019) are becoming more prevalent, the overall evidence of cause-and-effect mechanisms of different UFP's characteristics is still incomplete. The study by Schwarze et al. (2007) emphasized the significance of size and composition of the particles in their study and suggested that these characteristics of UFP could result in distinct cellular responses. A study by Juarez-Facio et al. (2022) applied standardized methods for the generation of UFP with different chemical compositions with two different operating conditions of mini Combustion Aerosol Standard (miniCAST), but the study emphasized the need for further optimization and regulated delivery, since cellular responses were not always observed.

The miniCAST soot generator (Jing, 1999) is one of the recognized combustion-derived aerosol sources. In a CAST, the soot is produced from a propane- diffusion flame that is continuously quenched by N_2. Changing the different settings/ operating conditions of the CAST allows changes in the physical and chemical properties of its emissions (Moallemi et al., 2019; Moore et al., 2014). This flame- derived soot generator, with different set parameters, has the potential to mimic soot of real-world extrapolations without after-treatment systems (Ngo et al., 2020). For example, a study by Moore et al. (2014) studied operating conditions of miniCAST where the generated soot particles behave as analogue to real-world aircraft and diesel engine sources concerning the OC fraction, soot mode size, concentration and hygroscopicity. Another study by Marhaba et al. (2019) showed that some miniCAST's operating conditions facilitates generation of soot particles similar to aircraft soot in terms of the internal nanostructure, morphology and chemical structure. The miniCAST was also used as a calibration aerosol source to act as a surrogate of engine exhaust emissions for the physicochemical and optical properties (Ess and Vasilatou, 2019).

In the present study a miniCAST was used to produce two types of reference UFP (high organic content and low organic content) with similar physical properties, continuing research on the biological effects of chemical soot particle composition after photochemical processing (Offer et al., n.d.; Pardo et al., 2022, 2023) but now focusing on variations in combustion by-products. Adenocarcinoma human alveolar A549 epithelial cells were exposed to both types of UFP, and the toxicological responses were studied, to investigate the influence of primary organic coating and particularly the PAH content of UFP on toxicity in a repeatable and reproducible *in vitro* system.

2. Materials and methods

2.1. Generation of the UFP reference aerosols

The UFP was generated with a miniature combustion aerosol standard soot generator (miniCAST, model 5201C; Jing ltd., Switzerland).

The miniCAST uses a stream of fuel (propane) where the oxidation air is fed coaxially, resulting in a diffusion flame (Jing, 1999). By quenching the flame with nitrogen, a very high number concentration of UFP rich in organics can be produced, internally diluted, and cooled to about 50 °C within the miniCAST (Malmborg et al., 2019). Flows were optimized for a fuel rich condition (lambda, λ= 0.80, Φ = 1.25) to produce UFP with high organic content. Flow rates of propane, quench N_2, dilution air and burner air were 0.055 L/min, 7 L/min, 20 L/min and 1.05 L/min, respectively. For all the experiments, the operating conditions of the miniCAST were kept constant. To reduce coagulation and formation of larger agglomerates, the miniCAST's exhaust was immediately diluted by a homebuilt porous tube diluter (PTD) with adjustable dilution ratio and an ejector diluter with fixed 1 in 10 dilution ratio (VKL 10; Palas, Germany). The dilution in the PTD was adjusted in the beginning of each experiment and slightly readjusted during the four-hour period of each experiment to achieve constant characteristics (particle number and mass concentrations) throughout the experiments. Different organic loading of the particles was achieved by passing the diluted UFP aerosol through a catalytic stripper ((CS), Model CS015; Catalytic Instruments, Germany) at different temperatures and a charcoal denuder. The CS, when heated to 350 °C removes the particle and gas phase semi volatile organic (SVOCs) fractions from the UFP. The diffusional losses within the CS used in this study were around 10 % for 50 nm particles (Swanson and Kittelson, 2010). In contrast, keeping the CS at a room temperature setting, there was no removal of SVOCs, from the UFP maintaining the organic load at a level higher than that of the UFP stripped at 350 °C. These temperature settings resulted in UFP with varying chemical loads (original at room temperature and stripped at 350 °C). To realize UFP-only exposures, the organic gas phase had to be removed in any case. Therefore, the CS was followed by a square multi-channeled charcoal denuder with 325 squared channels, 0.9 mm × 0.9 mm (Helsatech, Germany) to remove gas phase organics (Binder et al., 2022). Although particle losses of the charcoal denuder were lower compared to the CS, it was installed even when the CS was heated to keep possible artifacts and losses in the experiments with and without heating of the CS comparable. In the following these two UFP types were termed UFP-H (high organic load UFP) and UFP-L (low organic load UFP). After the denuders, the UFP were guided through a further dilution step applying a second 1 in 10 ejector diluter taking constantly 1.65 L/min. This was followed by different instruments for online characterization, collection of the UFP for offline aerosol characterization and cell exposure in the Automated Exposure System (AES, Vitrocell, GmbH, Germany).

A schematic of the experimental setup is presented in Fig. 1. To minimize particle losses and reactions throughout the entire setup, conductive perfluoro alkoxy (PFA) tubing material was used. This type of tubing material prevents the accumulation of static electric charges causing particle losses and therefore has a high transmission efficiency (Liu et al., 2019). PFA tubes were used with inner diameters of 4 mm or 10 mm (depending on the flow rates) to ensure laminar flow and

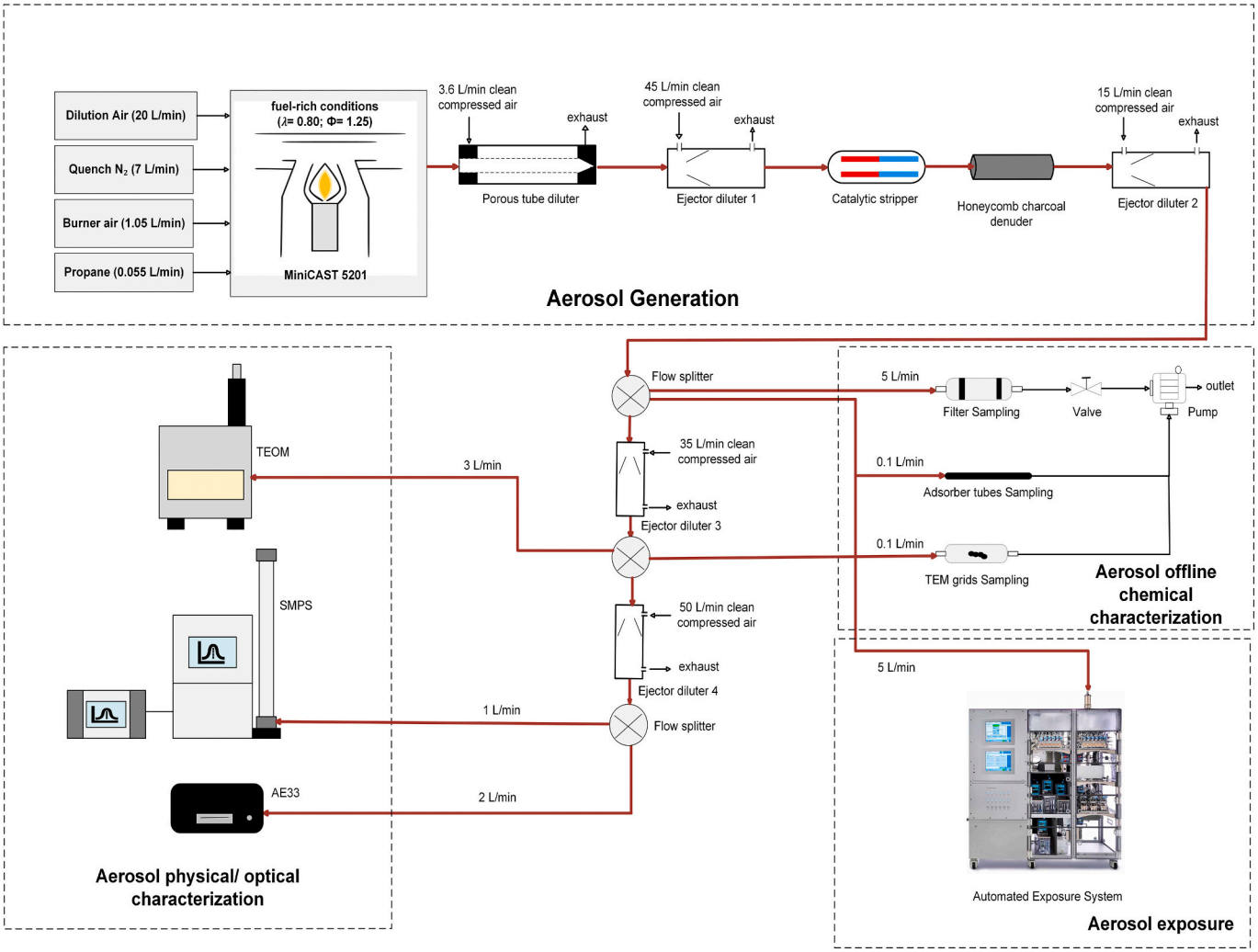

Fig. 1. Experimental set-up of soot generation, characterization, sampling methods and exposure in the ALI. TEOM - Tapered Element Oscillating Microbalance, SMPS - Scanning Mobility Particle sizer, AE33 – Aethalometer, TEM – Transmission Electron Microscopy.

minimize losses due to turbulence. All the instruments and the AES were operated nearby the miniCAST to reduce diffusion losses of UFP. Nevertheless, diffusional particle losses are unavoidable and coagulation during transport cannot be completely neglected.

2.2. Online characterization of the UFP reference aerosols

After appropriate further dilution (Fig. 1), the UFP was guided to the online instruments for investigating their physical characterization. A TSI Scanning Mobility Particle sizer (SMPS) (Type 3082 TSI Incorporated, USA) was used for determining the size distribution and geometric mean mobility diameter (GMD_{mob}). The size range selected for the SMPS was 5.94 nm to 224.7 nm with a sheath flow of 10 L/min and an aerosol flow of 1 L/min. A Tapered Element Oscillating Microbalance (TEOM 1400a, Ambient Particle Monitor, Rupprecht & Patashnick Co., Inc., USA) with a total flow of 3 L/min was used to measure the UFP mass concentration. A seven wavelengths dual spot Aethalometer (AE33 Aethalometer, Magee Scientific, USA) was installed to determine the equivalent black carbon mass concentration ((eBC,) (Petzold et al., 2013)) and the Absorption Ångström Exponent (AAE) (Liu et al., 2018) of the UFP. The aethalometer was used with a total aerosol flow of 2 L/min. The wavelength- independent multiple scattering correction factor, C = 1.39, as provided by the manufacturer for the built-in filter tape was utilized. The AAE was calculated using two pairs of wavelengths *i.e.* namely, AAE 470/ 950 and AAE 370/ 880 (Moosmüller et al., 2001; Perron et al., 2010; Segura et al., 2014; Zotter et al., 2017). The compensated aethalometer specific mass absorption cross sections (MAC) used at 370 nm, 470 nm, 880 nm, and 950 nm were 18.47 m^2/g, 14.54 m^2/g, 7.77 m^2/g, and 7.19 m^2/g respectively (Drinovec et al., 2015). The eBC was calculated from the conversion of the absorption coefficient (σ_{ab}) at 880 nm with its respective MAC (7.77 m^2/g).

2.3. Offline characterization of the UFP reference aerosols

2.3.1. Particulate matter (PM)

Quartz fiber filters (QFF, Ahlstrom Munksjö Ltd., Sweden) were used for filter sampling of the UFP. Before sampling the filters were preheated at 550 °C for 5 h. Filter samples were stored at −20 °C after each experiment until further analyzes. Field blanks were taken for corrections. Untargeted qualitative analysis of samples was carried out with a thermal desorption comprehensive two- dimensional gas chromatography hyphened with time-of-flight mass spectrometry (TD–GC × GC–TOFMS) on a Pegasus BT4D (LECO, USA) facilitated with an OPTIC-4 GC inlet system and a Cryofocus-4 cryogenic trapping system (GL Sciences, Netherlands). Circular filter punches of 2 mm in diameter were placed into a GC injection liner and thermally desorbed after being manually spiked with deuterated PAHs standards (1 μL of an internal standard (ISTD)). The chromatographic separation was done with a nonpolar capillary column (60 m, BPX5, SGE, Australia), installed in the first dimension and a midpolar capillary column (1.5 m, BPX50, SGE, Australia) in the second dimension (Table S1). The mass spectrometric analysis was done with electron ionization at 70 eV and detection by TOFMS. Details of the applied chromatographic and classification parameters for the analysis are provided in Tables S2 and S3 respectively. Further information on the inlet flow and temperature settings can be found in Tables S4 and S5 respectively. Targeted quantification of Polycyclic Aromatic Hydrocarbons (PAHs) was carried out by means of gas chromatography mass spectrometry (Shimadzu GCMS-QP2010 Ultra, DTD-20 Shimadzu, Japan). The analyzes were done with direct thermal desorption (DTD) (Orasche et al., 2011) using OPTIC-4 inlet (GL Sciences B.V., The Netherlands) of defined filter punches (d = 6 mm). The punches were manually spiked with deuterated PAHs standards (1 μL of an internal standard (ISTD)) prior to placing them in the GC injection liner. More details of the analytical procedure are described in (Schnelle-Kreis et al., 2005). For the quantification of the PAHs, each sample was measured at least twice for reproducibility of measurements.

Representative highly loaded QFF were analyzed by Raman micro spectroscopy (LabRAM (HR system, Horiba, Japan) (Bladt et al., 2014; Ess et al., 2016; Raiolo et al., 2024) using a laser excitation wavelength of 633 nm (0.1 mW at the sample) and a long working distance objective lens of 50× magnification (NA = 0.5). The focused laser beam was scanned over an area of 10 μm × 10 μm 800 1/cm to 2000 1/cm was recorded.

To study the morphology of the UFP, Transmission Electron Microscopy (TEM) grid samples were collected by directing a small volume (0.1 L/min) of the aerosol for 7.5 to 30 min through a perforated carbon film on a copper carrier mesh grid (200 mesh copper; Plano GmbH, Germany). The sampled grids were stored in a low humidity silica desiccator at room temperature prior analyzes with a Transmission Electron Microscope (TEM, JEM-2100F, JEOL Ltd., Japan) at 200 kV.

2.3.2. Gas phase

Adsorber tubes containing three sublayers of graphitized carbon black (GCB) sorbents were used for trapping compounds of different volatility (Gawlitta et al., 2023). Gas phase samples were collected in absorber tubes where a stainless-steel filter holder with a QFF was used upfront for removing the particulate fraction and protecting the adsorber tubes. Gilian GilAir Plus Personal Sampling Pumps (Gilian, USA) were used for sampling with a flow rate of 0.1 L/min to avoid breakthroughs of more volatile compounds. Field blanks were taken for corrections. The samples were stored at −20 °C after each experiment until further analyzes. Analyzes of the adsorber tubes were conducted by thermal desorption (TD) with a Shimadzu TD-20 thermal desorption unit (Shimadzu, Japan), coupled to a gas chromatography hyphened mass spectrometry system (Shimadzu GCMS-QP2010 Ultra, Shimadzu, Japan). The analyzes of the samples were done as per (Gawlitta et al., 2023; Mason et al., 2020) where the samples were spiked with an isotope- labelled standard mixture before analyses.

2.4. Cell culture, seeding and aerosol exposure

Human alveolar epithelial A549 cells (ACC 107, Leibniz Institute DSMZ - German Collection of Microorganisms and Cell Cultures, Germany) were cultured in high-glucose Gibco Dulbecco's Modified Eagle Medium consisting of Nutrient Mixture F-12 (DMEM/F-12; LIFE Technologies, 31,331,093, USA) supplemented with 5 % (v/v) fetal bovine serum (FBS; LIFE Technologies, 10,500,064, USA), 100 U/mL penicillin, and 100 μg/mL streptomycin (P/S; Sigma-Aldrich, P4333, USA) in a humidified incubator at 37 °C and 5 % CO_2. Two days before exposure, A549 cells were seeded on the apical side of semipermeable transwell inserts (polyethylene terephthalate, 0.4 μm pore size, 4.67 cm^2 membrane growth area, Corning, USA) at a cell density of 64,000 cells/cm^2 growth area in DMEM/F-12 (5 % FBS). The day after, cells were set to the ALI by removing the medium from the apical side.

On the day of exposure, A549 cells reached near confluence and inserts were transferred to an automated exposure system (AES, Vitrocell, Germany). The system was used to expose A549 cells at ALI for 4 h to the generated UFP aerosols, conditioned to a relative humidity (r.H.) of 85 % at 37 °C at a flow rate of 100 mL/min over each exposure unit as previously described (Mülhopt et al., 2016; Oeder et al., 2015). One module was used as clean air (CA) control (100 mL/min of purified air at 85 % rH. per unit). The size-dependent deposition of particles in the ALI exposure system was estimated from the SMPS data using the methodology outlined by Lucci et al. (2018). The basolateral exposure medium consisted of serum-free DMEM/F-12 GlutaMAX medium supplemented with 1 % P/S and 15 mM N-2-hydroxyethyl piperazine-N-2-ethane sulfonic acid buffer solution (HEPES, ThermoFisher Scientific, 15,630–056, USA). Incubator (Inc) control inserts served as control for the impact of the AES and airflow exposures were kept in an incubator free of CO_2 during the exposure period. After the exposure, cells were used for direct analysis and the exposure medium was collected in aliquots and frozen at −80 °C for later analysis.

2.5. Cytotoxicity and cell viability

After 4 h of exposure, different cellular assays and analysis were carried out in a minimum of three independent experiments for both UFP (UFP-H and UFP-L).

Cytotoxicity was evaluated by measuring the Lactate dehydrogenase (LDH) release by the Cytotoxicity Detection KitPlus (L-LDH; Roche, 11,644,793,001, Switzerland). The cell exposure media directly collected after the exposure from the basolateral side of the insert were analyzed to measure the amount of LDH released upon plasma membrane damage. Serum-free exposure medium acted as blank. LDH released by negative control cells treated with a 2 % Triton™ X-100 (Sigma-Aldrich, Germany) solution for 20 min served as positive control (PC). The LDH kit was used according to the manufacturer's instructions. The LDH released by the cells was assessed by measuring the absorbance at 493 nm with a Varioskan™ LUX multimode microplate reader (Thermo Scientific, USA). The results are shown as % of LDH maximal release (cytotoxicity) ± standard error of the mean (s.e.m) of N independent experiments (s.e.m, $N = 3$).

Cell viability was assessed by the resazurin assay. After exposure, cells were washed with phosphate buffered saline (PBS) and 10 % PrestoBlue HS Cell Viability Reagent (ThermoFisher Scientific, A13262) in serum-free DMEM/F-12 was added to the apical and basolateral compartment. Following an incubation time of one hour, 200 μL aliquots of the solution were pipetted into a 96-well plate, and the metabolic activity of cells was analyzed with a microplate reader by measuring the fluorescence at 570 nm (Varioskan LUX, ThermoFisher Scientific). The results are shown as % cell viability ± s.e.m. ($N = 3$).

2.6. Oxidative stress markers

The induction of oxidative stress after aerosol exposure was assessed by measuring the release of malondialdehyde (MDA), an end-product of lipid peroxidation, in the basolateral medium. MDA levels were quantified as previously described (Cao et al., 2022) from the collected basolateral exposure media by using liquid chromatography (LC) tandem mass spectrometry (API 4000, AB SCIEX, USA) in positive MRM mode. MDA was derivatized with 2,4-Dinitrophenylhydrazine (DNPH; Sigma–Aldrich, 04732) and extracted by liquid-liquid extraction and subsequent chromatographic separation on a C18 column (Agilent 1290 UHPLC System) applying isocratic conditions. Results are presented as MDA ng/mL ± s.e.m. ($N = 3$).

Reduced and oxidized forms of glutathione are generally used to assess the oxidative condition of a biological system and were quantified by adapting methods previously described (Herzog et al., 2019; Sun et al., 2020) using LC-MS/MS. Directly after 4 h exposure, cells were washed twice with an ice-cold 1 mM N-ethylmaleimide (NEM; Sigma-Aldrich, E3876) solution in DPBS in the apical and the basolateral compartment. Throughout the whole sample preparation, samples were kept on ice. After aspiration, a precipitation solution of 20 mM NEM in absolute methanol was added to both compartments, followed by the addition of an internal standard mixture of labelled reduced (GSH, 6.5 mM; Sigma-Aldrich, 683,620) and oxidized glutathione (GSSG, 67 μM) to the apical side. The labelled oxidized glutathione was synthesized as described in Herzog et al. (2019). Cells were incubated for 5 min and harvested by scraping. Since a leakage of extraction solution through the membrane cannot be excluded, supernatants of both compartments were combined, thoroughly vortexed and centrifuged at 10,000 x*g* for 7 min at 4 °C. The supernatant was then transferred to a new tube and the solvent evaporated under a nitrogen stream at 45 °C. Subsequently, precipitants were re-suspended in 100 μL of the mobile phase A (0.1 % formic acid; Promochem, SO-9679-B001; in H_2O). Samples were analyzed by LC-MS/MS in positive MRM mode on an Agilent 1260 HPLC system coupled to an Agilent 6470 tandem mass spectrometer. To assess GSSG concentrations 5 μL of the extract was injected to the HPLC system. The latter was equipped with a C18 column (Penomenex Kinetex 100 × 2.1 mm) and run with a gradient elution program (mobile phase A: 0.1 % formic acid and B: methanol) at 20 °C column oven temperature. For quantification of alkylated glutathione (GS-NEM) a 100-x dilution step was applied before injection of the extract to achieve concentrations in the linear calibration range of the instrument. Results are presented as % GSSG ± s.e.m. ($N = 3$).

The conversion of 2′,7′-dichlorodihydrofluorescein diacetate (H2DCF-DA) to the oxidized highly fluorescent dichlorofluorescein (DCF) was used to investigate the generation of intracellular reactive oxygen species (ROS). To do so, after aerosol exposure, cell inserts were washed twice with HBSS (ThermoFisher Scientific, 14,025,100) from both sides and 500 μL of 10 μM H2DCF-DA (Sigma-Aldrich, 287,810) solution in HBSS was added to the apical side. Cells were incubated at 37 °C for 30 min in the incubator (r.h. of 85 %, 5 % CO_2) and subsequently washed with HBSS. Afterwards, cells were lysed by scraping in 90 % DMSO in HBSS and collected in tubes. The latter were centrifuged at 10,000 ×*g* for 5 min at 4 °C and the supernatant was transferred in 120 μL aliquots to a black 96-well plate. The fluorescence of the oxidized DCF was measured at ex/em 485/535 nm in a microplate reader (Varioskan LUX, ThermoFisher Scientific). The Relative Fluorescence Unit (RFU) were normalized by using the metabolic cell equivalents derived from the corresponding LDH data (Heinrich et al., 2014; Romano et al., 2023). Results are presented as intracellular ROS normalized by the metabolic cell equivalent (MCE) ± s.e.m. ($N = 3$).

2.7. Cytochrome P450 activities

CYP1-dependent ethoxyresorufin-O-deethylase (EROD) and 7-Benzyloxyresorufin-O-dealkylase (BROD) activity was investigated by a treatment of cells with the fluorometric substrates 7-ethoxyresorufin or 7-resorufin benzyl after the four- hour exposures. Firstly, cells were harvested by trypsinization using 0.05 % Trypsin-EDTA solution (Sigma-Aldrich, MFCD00130286), transferred to a 96-well plate, and stored for lysis at −80 °C overnight. Two separate 10 μM reaction mixtures were prepared containing 7-ethoxyresorufin (Cayman, 16,122) or resorufin ethyl ether (Biomol, ABD-15023) in 0.1 % Triton-X to measure EROD and BROD activity, respectively. Afterwards, cells were thawed and incubated with the reaction mixtures for 5 min at 37 °C (r.h. of 85 %, 5 % CO_2). Subsequently, the activation solution containing 1 mM NADPH (Applichem, A1395,0100) in H_2O was incubated for another 10 min at 37 °C. A calibration curve of resorufin (Cayman, 700,023) was added to precisely determine the enzyme concentration. The fluorescence of resorufin was measured at ex/em of 544/595 nm in a microplate reader (Varioskan LUX, ThermoFisher Scientific). Results are presented as activity of EROD and BROD normalized by the MCE ± s.e.m. ($N = 3$).

2.8. DNA damage

DNA single and double strand breaks were investigated by the alkaline version of single cell gel electrophoresis, also known as comet assay. After exposure, cells were washed once with HBSS and trypsinized with 0.25 % Trypsin-EDTA solution. Cells were counted and diluted to a cell density of 250,000 cells/mL with DMEM/F12 + 10 % FBS. From the cell suspension aliquots, the mini-gel version of the comet assay was conducted as previously described (Di Bucchianico et al., 2017). Cells treated with 30 μM H_2O_2 (Merck Millipore 107,209) served as positive control. Moreover, to analyze the amount of oxidative DNA damage, gels of additional slides were treated with the enzyme DNA-formamidopyrimidine glycosylase (Fpg; 4040_100_FM, Trevigen) after lysis as previously described (Di Bucchianico et al., 2017). Following electrophoresis, gels were neutralized using 0.4 M TRIS (Carl Roth, Karlsruhe, Germany, A411.1) and washed with ultrapure water. Slides were air-dried and stained with SYBR™ Green I Nucleic Acid Gel Stain (Invitrogen, S7563). Micrographs were taken with the Lionheart FX automated microscope in 20× magnification. 100 nucleoids per microgel were scored manually using the CometScore 2.0 (TriTek Corp)

software. Results are presented as % DNA in tail ± s.e.m. ($N = 3$).

2.9. Stability during biological exposures and statistical analysis

To assess the stability of UFP-H and UFP-L generation, the variability of the physical characteristics within the 4 h biological exposures were assessed by the coefficient of variation (CV). The CV was calculated as the standard deviation of the respective measured variable during a 4-h experiment divided by the average of that experiment and expressed as a percentage. The GMD_{mob}, PNC, MC, eBC, and AAE (470/950) (370/880) were considered for determining the stability of the UFP characteristics produced. For A549 toxicity testing, statistical analysis was performed using GraphPad Prism software version 9.0.0 by one-way analysis of variance followed by the multiple comparison Dunnett's test.

2.10. Repeatability of the UFP and statistical analysis

Over the course of more than a year, three separate measurement campaigns lasting several weeks with typically one experiment per working day were carried out (Table S6). The independent experiments for UFP-H were $N = 11$ (group A), $N = 5$ (group B) and N = 5 (group C), while for UFP-L were $N = 8$ (group A), $N = 4$ (group B) and N = 3 (group C). The repeatability of the generation of the UFP was assessed using results from these different campaigns. The repeatability of physical and optical properties for UFP-H and UFP-L within each measurement campaign was assessed by comparing the mean and standard deviations (Table S7). Welch's ANOVA test was done between the aerosol physical properties between the different groups (Group A, Group B and Group C) to ascertain if the averages of the groups were significantly different to one another. Depending on the probability (p) values obtained (<0.05), the Bonferroni correction was applied to adjust the p- values. The fold changes between each characteristic between the groups were also calculated by the ratio of the averages. All the tests were performed in the programming environment R (Version 4.3.1) using the interface of RStudio (Version 2023.06.1, Build 524) at $\alpha = 0.05$ (Tables S8 and S9).

3. Results and discussions

3.1. Characterization of the generated UFP reference aerosols

For this study two different UFP reference aerosols namely UFP-H (high organic load) and UFP-L (low organic load) were generated with similar physical (Table 1) but different chemical characteristics.

The number size distributions for UFP-H and UFP-L were similar and unimodal with a GMD_{mob} of about 40 nm (Fig. 2, I). The mass size distribution for UFP-H and UFP-L were also very similar (Fig. S1) The slightly lower GMD_{mob} of UFP-L may be explained by the stripping of organics from the soot aggregates as the CS removes a significant portion of the semi-volatiles and volatiles. With the use of the higher temperature in the CS for the UFP-L, the losses in the smaller size ranges might increase, which was adjusted by decreasing the dilution in the PTD to maintain similar particle number size concentrations. This could have resulted in an increment in the standard deviations of the size distributions. The mass concentrations measured by the TEOM for UFP-H and UFP-L were in a comparable range with a slightly lower value for UFP-L as seen for GMD_{mob}. The mass concentrations for both the UFP were

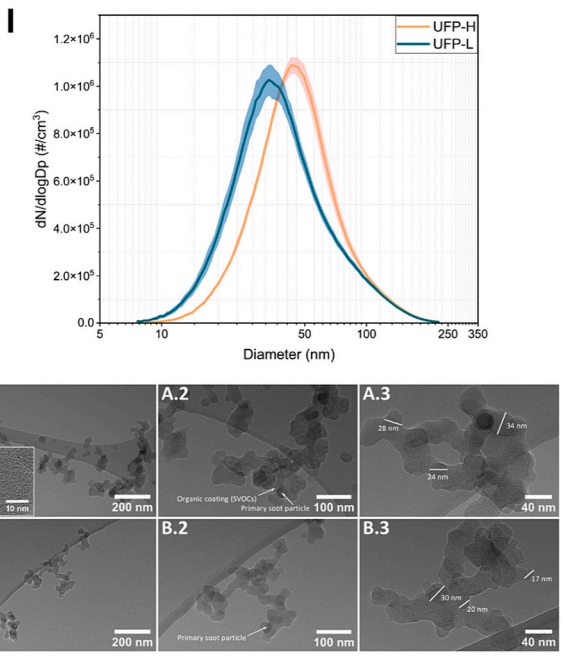

Fig. 2. (I) Size distribution of UFP-H and UFP-L. The shaded area represents the standard deviation of the number concentration (#/cm^3) in each size bins. (II) Fig. 5. TEM images: A.1 UFP- H showing the graphitic structure, magnification at 50,000×; A.2 UFP-H showing the primary soot particle and coating of SVOCs, magnification at 100,000×; A.3 UFP-H magnification at 200,000×; B.1 UFP- L magnification at 50,000×; B.2 UFP-L showing the primary soot particle; B.3 UFP-L magnification at 200,000×.

cross-checked using the SMPS (assuming a density of 1 g/cm^3) which gave the values of 80 μg/m^3 for UFP-H and 70 μg/m^3 for UFP-L.

The AAE is an important optical property of aerosol used for its characterization that describes the variation of wavelength dependence in light absorption (Liu et al., 2018). AAE is a specific property of each aerosol species where Black carbon (BC) has an AAE of around 1.0. Larger AAE values generally indicate an increase of organic content in the aerosol, due to both the presence of light-absorbing compounds in the organic aerosol and the internal mixing of black carbon and organics, leading to soot core-shell structures that enhance AAE (Virkkula, 2021). For the UFP generated in our setup, the AAE values ranged from 1.7 (UFP-L) to 2.0 (UFP-H) for both wavelength pairs. The high AAE values are an indication of high levels of aromatic structures (Samburova et al., 2016) present in the miniCAST generated UFP. The reduction of AAE from 2.0 (UFP-H) to 1.7 (UFP-L) indicates a decrease in organic content by the CS. The calculated eBC was higher for UFP-L than UFP-H. This increase might be due to an overestimation of using the same MAC values (7.77 m^2/g at 880 nm as provided in the AE33 manual) for both types of UFP soot generated. A study by (Romshoo et al., 2022) showed that thermally treated miniCAST soot with a size below 100 nm can have smaller MAC values of about 4.5 m^2/g. Therefore, while interpreting the eBC, uncertainties of MAC values should always be considered.

Offline chemical characterization was done from the particle phase

Table 1
Mass concentration (μg/m3), Particle number concentration (PNC) (#/cm3), Geometric mean diameter (GMDmob) (nm), Absorption Ångström Exponent (AAE) (470/950), AAE (370/880), equivalent black carbon (eBC) (μg/m3) and deposition of UFP-H and UFP- L. The results are represented as four-hour averages ± standard deviation on the averages of each experiment in group *A*.

Type	Mass concentration (μg/m^3)	PNC (#/cm^3)	GMD_{mob} (nm)	AAE (470/950)	AAE (370/880)	eBC (μg/m^3)	Deposition (ng/cm^2)
UFP- H (N = 11)	110 ± 10	50*10^4 ± 2*10^4	45 ± 1	2.0 ± 0.1	2.0 ± 0.1	47 ± 2	1.5 ± 0.2
UFP- L (N = 8)	90 ± 10	50*10^4 ± 3*10^4	40 ± 1	1.7 ± 0.0	1.7 ± 0.0	51 ± 3	1.4 ± 0.2

samples on QFF and gas phase samples in adsorber tubes for both UFP aerosols. Firstly, an untargeted screening of the particle phase samples of UFP-H and UFP-L was done using GC × GC-ToFMS. Fig. 3 displays the bubble plots of the significant peaks obtained in the chromatograms after the analyzes of UFP-H (top) and UFP-L (bottom). Significantly higher amounts of PAHs with *m/z* 178–300 were found in UFP-H compared to UFP-L including parent and alkylated four-, five- and six-member ring PAHs. Only for UFP-H, oxygenated PAHs were detected in a comparably low concentration. Similar results were published by (Schneider et al., 2022) regarding higher PAH content for UFP-H from group A by application of Electron Spray Ionization-Fourier-Transform Ion Cyclotron Resonance Mass Spectrometry (ESI-FTICRMS). The authors stated the presence of larger PAHs (≥ 6 rings) with an m/z up to 800. These compounds are not detectable by our measurements as it is far beyond the volatility range that can be covered by GC × GC-ToFMS. Only low amounts of Phenanthrene, Pyrene and Benz(*a*)anthracene can be detected for the UFP-L sample after correction by a measurement of a purified air sample. Sections of the original chromatograms of UFP-H, UFP-L and purified air can be found in the supplementary (Fig. S2) as well as the classification of compounds found in UFP-H and UFP-L (Table S10).

Of the sixteen designated High Priority PAHs by the Environmental Protection Agency (EPA) (Hussar et al., 2012), eleven mainly particle bound PAHs (≥5 aromatic rings) and two intermediate PAHs (3–4 aromatic rings) were quantified for UFP-H and UFP-L in a targeted analyzes by direct thermal desorption hyphened gas chromatography mass spectrometry (DTD-GCMS). The PAHs in UFP-H constituted approximately 2.5 % of the total UFP mass, signifying high PAHs concentrations including benzo[*a*]pyrene, which is considered one of the most toxic PAHs that has been thoroughly characterized in terms of its toxicity (Jung et al., 2010). The content of Benzo[*a*]pyrene was analyzed to be of about 2 mg per g UFP total mass. Fig. 4 shows the concentrations at ALI for all targeted PAHs. A semi-quantitative study by (Ngo et al., 2020), using a miniCAST exhaust without a CS had similar observations where they found mainly semi- volatiles (m/z 176–242) and non- volatiles (m/z ≥ 252) formed at a lambda of 0.805 and negligible amounts of volatiles (m/z 78–166). The targeted nonvolatile PAHs in UFP-L were always below the limits of quantification (LOQ) of 0.01 ng/m^3.

The Raman spectra of soot, which is used to study its nanostructure, exhibit two prominent overlapping bands at approximately 1350 1/cm (D or 'defect') and 1600 1/cm (G or 'graphite') (Cuesta et al., 1994; Tuinstra and Koenig, 1970). Two exemplary spectrums of UFP-H and UFP-L for Group A is shown in Fig. S3. According to (Ferrari and Robertson, 2000), the increase in the height-ratio I(D)/I(G) is linked to an increase in structural order for amorphous and disordered carbons, hence lower I(D)/I(G) values indicate more amorphous structures and can be expected for soot samples with higher organic carbon (OC) content. The found I(D)/I(G) ratios for the UFP-H and UFP-L were 0.99 ± 0.05 (N = 3) and 1.05 ± 0.02 (N = 3), respectively. These values indicate very similar structural order with slightly higher amount of

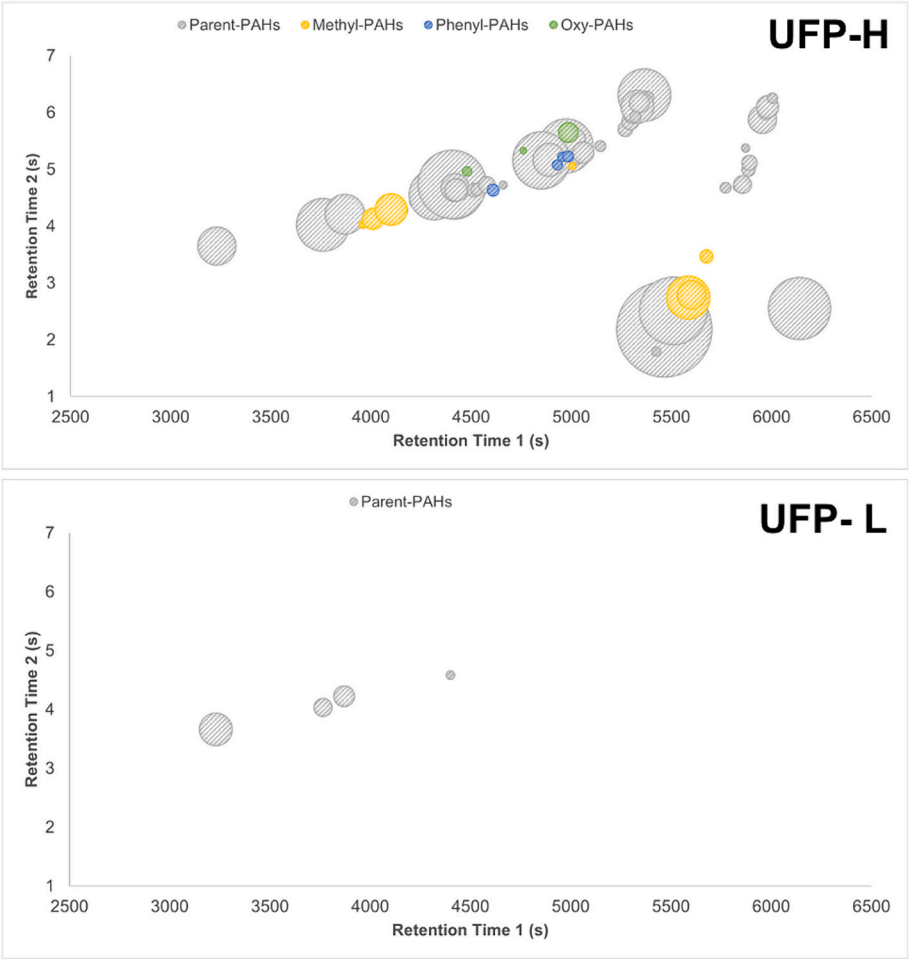

Fig. 3. Chemical characterization of UFP-H (top) and UFP- L (bottom) *via* DTD-GC × GC-TOFMS. PAH content of the two samples is shown along the two-dimensional separation space. The peak area is represented by the diameter of the "bubble". Plots are normalized to the area of the most abundant PAH found in UFP-H. Both samples were corrected by a purified air measurement. Methyl-PAHs: Methylated PAHs, Phenyl- PAHs: Phenylated PAHs, Oxy-PAHs: Oxygenated PAHs.

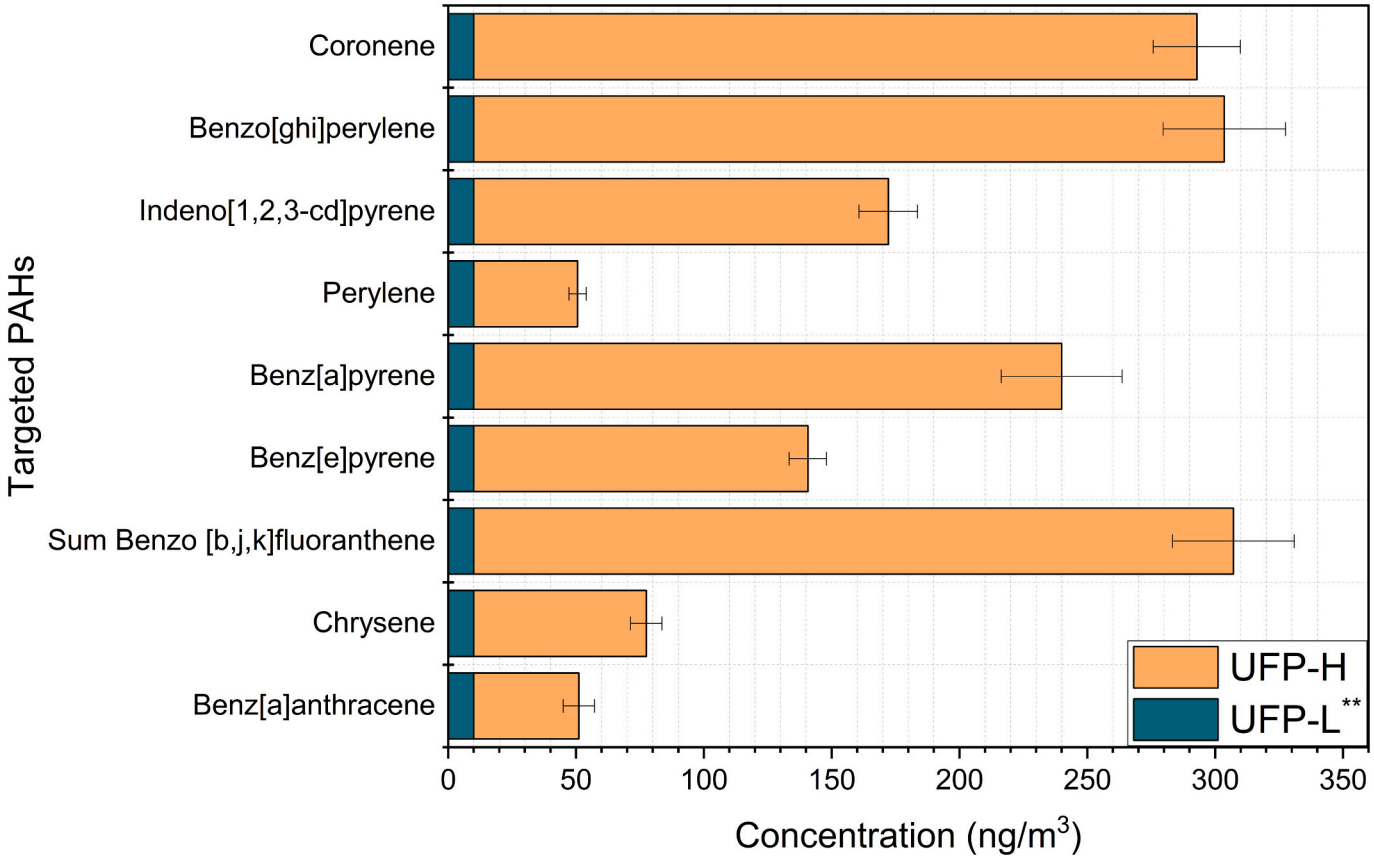

Fig. 4. Concentration of polycyclic aromatic hydrocarbons (PAHs) in UFP-H ($N = 7$). The error bars represent the standard deviation of each targeted PAHs in all the experiments. ** The analyses for the UFP-L samples were all under the limit of quantification (LOQ). The LOQ for our method is 0.01 ng/m^3.

amorphous carbon for UFP-H. This agrees with the results found by (Ess et al., 2016) where the lowest OC soot (4 %) had the highest I(D)/I(G) of 1.19 ± 0.02 and the highest OC soot (47 %) had the lowest I(D)/I(G) of 1.03 ± 0.03.

To compare the morphology and to determine the degree to which thermal treatment in the catalytic stripper altered the structure of the UFP, samples were collected and analyzed using a TEM (Fig. 2, II). Both UFP showed soot agglomerates with primary particles consisting of graphitic-layered structures. These structures are comparable to soot from other combustion sources like diesel soot (Vander Wal et al., 2007; Vander Wal and Tomasek, 2004). The fractal aggregates of both UFP were similar and clearly did not change with thermal treatment. A geometric primary particle size of 22 ± 6 nm was determined for UFP-H ($N = 54$) and 22 ± 6 nm for UFP-L ($N = 39$). Similar observations are in accordance with particle data from (Ess et al., 2021) for near-stoichiometric diffusion flame with a miniCAST burner. Though the size of the primary particles were very similar to each other, a more amorphous appearance with blurry boundaries between the primary particles was observed for UFP-H indicating a considerable amount semi volatile species.

For a thorough comparison of the UFP-H and UFP-L, it is essential to consider the gas phase. Therefore, four volatile compounds namely 2-Methylnaphthalene, 1-Methylnaphthalene, Biphenyl and 1,2-Dimethylnaphthalene were quantified using a targeted TD- GC- MS for both UFP. Contrary to the concentration differences for the PAHs in the particle phase, no significant differences in the gas phase for UFP-H and UFP-L were observed (Table S11). Although PFA was used as tubing material, the similar concentration of gas phase compounds for both UFP types indicates a strong carryover from previous UFP-H experiments and needs to be considered in future research that includes the effects of gas phase compounds in PM toxicological studies.

3.2. Toxicological assessments

The two aerosols, UFP-H and UFP-L were investigated for their toxic potential in human alveolar epithelial ATII cells (A549) exposed at the ALI (Fig. 5). In our study, the calculated deposition of UFP mass per area was similar for UFP-H and UFP-L (Table 1).

Cytotoxicity was assessed by measuring the LDH release into the basolateral exposure medium, which occurs upon rupture of cell membranes, a hallmark of necrosis cell death. Both aerosols induced a significant cytotoxic response to the same extent (≈27 %) compared to the clean air (CA) control (Fig. 5, I). Comparable results could be observed for the cell viability analysis, in which both aerosols reduced the cellular metabolic activity to 56 % (UFP-H) or 50 % (UFP-L) of the incubator control, and displayed a significant decrease compared to the CA control (82 %) (Fig. 5, II). Our results indicate the capacity of UFPs to cause necrosis, a well-known cause of inflammation, *via* the release of danger signal which can activate the NLRP3 inflammasome, a multiprotein complex involved in the regulation of inflammation (Øvrevik et al., 2015). Generally, it was already observed in previous studies that UFP can induce an impairment of cell viability and metabolism, although in higher concentrations than applied in our study (Andreau et al., 2012; Hammond et al., 2022; Salinas et al., 2020). Nevertheless, previous studies (Bonetta et al., 2009; Borgie et al., 2015; Hammond et al., 2022) demonstrate that the mechanisms of toxicity are strongly dependent on the chemical composition of the aerosol, which is usually neglected for the elaboration of limit values. Even though the cytotoxicity assessment did not show clear differences between the two UFP, an in-depth analysis was conducted aiming to unravel the influence of UFP's chemical composition on the oxidative stress response, xenobiotic metabolism, and genotoxicity of the exposed cells. Following 4-h exposure, particles with low amounts of organic content caused a significant oxidative

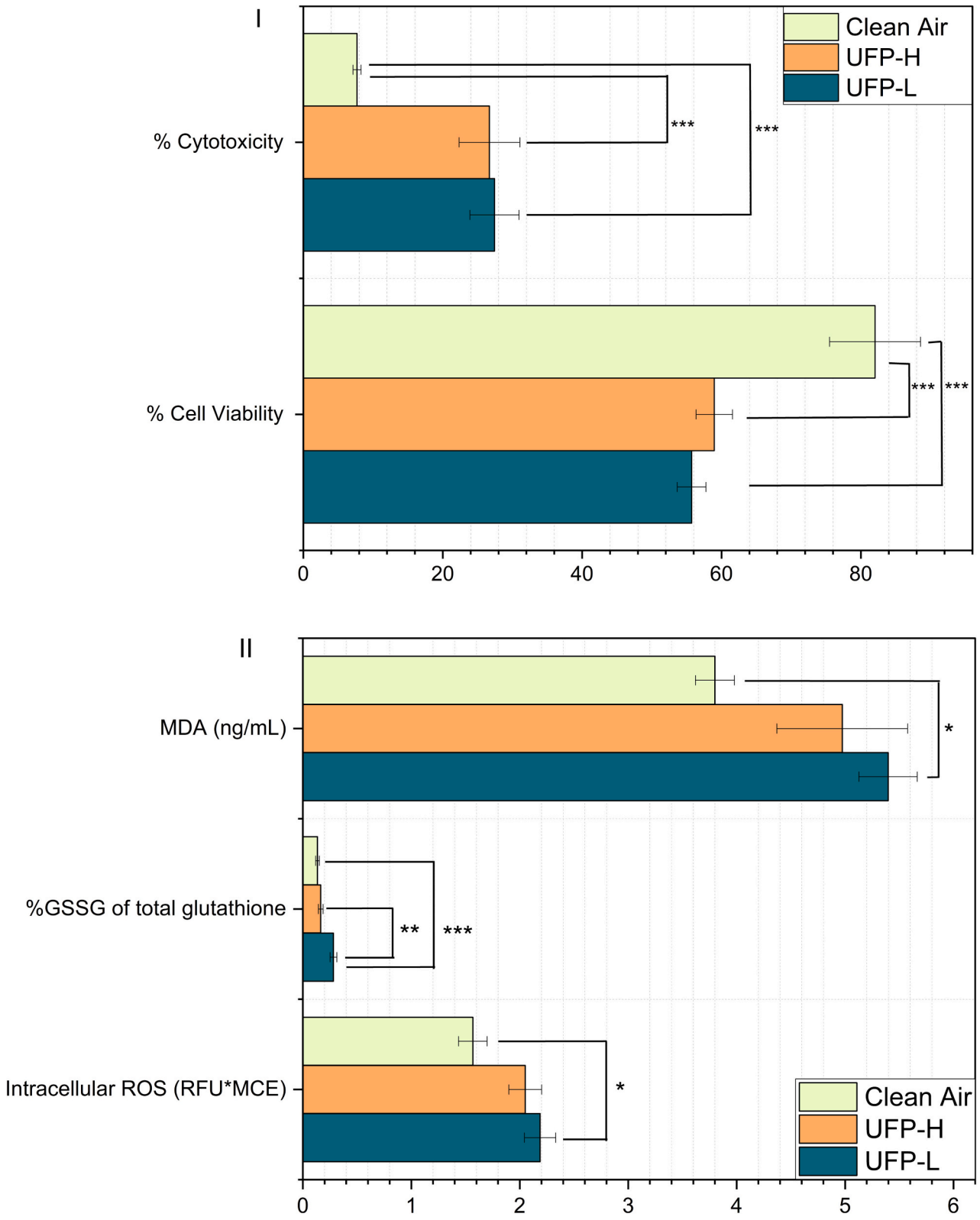

Fig. 5. Cell Viability and Oxidative Stress. The percentage of cytotoxicity measured by LDH release in cell medium following 4 h exposure and percentage of cell viability measured by the resazurin assay following 4 h exposure of A549 cells (I) The potential of oxidative stress was investigated by the detection of MDA [ng/mL] released into the sample medium, the percentage of intracellular oxidized glutathione (GSSG) of the total glutathione, as well as the formation of intracellular ROS (RFU*MCE) following 4 h exposure of A549 cells. (II) UFP-H, ultrafine particles condensed with high amounts of semi-volatile organic compounds; UFP-L, ultrafine particles condensed with low amounts of semi-volatile organic compounds. Bars represent the average ± s.e.m. ($N = 3$). Statistically significant results with respect to CA are marked with asterisks (*, $p < 0.05$; **, $p < 0.01$; ***, $p < 0.001$).

stress response in epithelial cells, while exposure to particles bearing high amounts of organic content led to a non-significant, but slight induction of oxidative stress markers. Compared to the CA controls, especially UFP-L triggered an intracellular generation of reactive oxygen species (ROS; Fig. 5, II), which seems to be partially scavenged by the GSH antioxidant system as indicated by increased levels of GSSG (Fig. 5, II). Nevertheless, the elevated GSSG levels could also indicate a decreased enzymatic activity of oxidative stress enzymes such as glutathione reductase responsible for the recycling of GSSG to GSH, which has been proposed before as a mechanism of ambie nt PM toxicity (Hatzis et al., 2006). GSH regulation has shown to play an important role in pro-inflammatory processes in the lung and an imbalance of the oxidant/antioxidant capacities can be associated with diseases such as cystic fibrosis or asthma (Rahman and MacNee, 2000), there is already a link between oxidative stress and inflammation in the lung and lung diseases. Moreover, slightly increased levels of the lipid peroxidation marker, MDA were detected to a similar extent for both UFP (Fig. 5, II), which could additionally indicate an imbalance and overloading of the antioxidative defence systems leading to the oxidation of macromolecules such as phospholipids, a main constituent of the cell membrane (Tsikas, 2017). The exposure to UFP-H induced a significant increase in EROD activity and a slight increase in BROD activity (Fig. 6, I), indicating enhanced enzymatic activity of CYP 450 monooxygenases, such as the phase metabolism enzymes CYP1A1 (Borgie et al., 2015; Shimada and Fujii-Kuriyama, 2004; Wohak et al., 2016) or CYP3A4 (Oeder et al., 2015). The latter is commonly known to be activated by PAHs such as benzo[*a*]pyrene or benzofluoranthenes (Genies et al., 2013; Wohak et al., 2016) as prevalent in UFP-H. Investigated monooxygenases were not induced by UFP-L, further supporting the assumption that two chemically different aerosols were produced. Different responses between UFP-H and UFP-L exposure could also be observed in the DNA damage analysis (Fig. 6, II). Although both types of UFP induced DNA strand breaks, with UFP-L to a greater extent than UFP-H, particles with high levels of organic content appear to promote DNA modifications that are recognized by the base excision repair enzyme Fpg (Fig. 6, II). These findings are in accordance with previous studies showing a correlation between increased levels of Fpg-sensitive sites and PAH exposure (Andersen et al., 2018; Genies et al., 2013).

3.3. Stability, repeatability and statistical analysis

The coefficient of variation (CV) was determined for each experiment of UFP-H and UFP-L for the four- hours of exposure to ascertain the stability of the generated UFP. The CV was <15 % in all experiments and all three campaigns indicating stable generation of the UFP-H and UFP-L. The repeatability of the UFP-H and UFP-L generation was assessed by comparing the mean and standard deviations (Table S7) of the different properties measured by the different aerosol characterization instruments for the separate measurement campaigns (Group B and Group C). The online instruments showed comparable results indicating a reproducible generation of the UFP. However, higher concentrations of all PAHs were observed in the separate measurement campaign (Fig. S4, A). But no change in pattern could be observed after normalizing to the total concentration of PAHs (Fig. S4, B). Therefore, we suspect that less particle losses occurred in Group B where our filter sampler was located closer to the miniCAST (*ca.* 5 m) contrary to the other groups (Group A, Group C) where the distance was about 20 m. To verify this and to characterize the process of particle losses in longer lines, additional experiments with similar settings were conducted. Here, measurements of size distribution were done in parallel after a 5- and a 20-m -long tubing (Fig. S5). These results suggested similar factors of loss of the UFP mass and PAHs with increasing sampling line length. Therefore, a strong scrutiny of the distance of sampling units should always be done before doing experimental setups, particularly for UFP.

Welch's ANOVA could not reject the hypothesis on similar Groups A, B, and C for the AAE370/880's of both UFP-H and UFP-L. For PM mass concentration, PNC, GMD_{mob} and eBC in both UFP-H and UFP-L, the Bonferroni correction was applied after rejection of the null hypothesis by Welch-ANOVA for *post hoc* testing. For UFP-H, none of the group's differences in means was significant except for mass concentration (Group A and Group B), GMD_{mob} (Group A and Group B; Group A and Group C) and eBC (Group A and Group C). However, except for eBC, the fold changes of the aerosol properties between these groups were ≈1, indicating small differences between the group means. Therefore, significant differences are a consequence of the high reproducibility within the individual groups. The same holds for UFP- L, where most of the significantly different means (for mass concentration, number concentration, GMD_{mob} and eBC) that appeared between Group A and Group B were statistically different ($p < 0.05$). For both UFP-H and UFP-L, eBC was significantly about 20–30 % lower in Group A than in the other two Groups B and C. Although mass concentration, eBC depends on the inherent carbon structure of the soot, determining its absorption properties. Since both mass and number concentration of particles show fold changes closer to one than eBC, it points to uncertainty related to the eBC quantification.

4. Conclusions

We generated two different UFP reference aerosols using a miniCAST generator with appropriate set points and dilutions. By treating the aerosols with a catalytic stripper at different temperatures and a charcoal denuder, UFP with distinct content of semi volatile organic compounds (UFP-H and UFP-L) but similar physical properties were generated. A variety of techniques, including a Scanning Mobility Particle sizer (SMPS), Transmission Electron Microscopy (TEM), two-dimensional gas chromatography hyphened with time-of-flight mass spectrometry (TD–GC × GC–TOFMS), Targeted quantification by direct thermal desorption hyphened gas chromatography hyphened mass spectrometry (DTD-GC–MS) were used to appropriately characterize the physical and chemical properties of these UFP. PM and gas phase sampling and analysis was carried out for characterization of the aerosol composition. The reference aerosols were used and characterized in three independent campaigns, demonstrating that the physical properties (mass concentration, PNC, GMD_{mob}, eBC, AAE) can be determined with a high degree of reliability and repeatability. The investigation of the composition and concentration of the UFP showed that long sampling lines can lead to significant particle losses, which was identified as the main driver of experimental variance for UFP among the three independent campaigns.

Human alveolar A549 adenocarcinoma cells were exposed to both types of UFP, and various toxicological responses were studied. Exposure to the different UFP led to the activation of distinct biological effects. The cytotoxicity assays carried out showed similar responses for both UFP-H and UFP-L exposures. The intracellular generation of ROS was significantly higher for UFP-L than for UFP-H while the activation of xenobiotic metabolizing enzymes was significantly higher for UFP-H. This suggests that the UFP differences in organic content induce different biological responses.

The UFP was produced during multiple campaigns and thus demonstrates the applicability of this method. Each exposure experiment took four- hours to complete and required constant and stable UFP production. The biological replicates for every campaign required redundant exposures, and the UFP were reproducibly produced where the daily variability remained low and stable throughout the campaign. In addition, the variations in the reference UFP parameters during annually repeated campaigns were also small, indicating that the UFP generation of aerosols was repeatable.

Our work highlights a method to produce UFP with similar physical and different chemical characteristics for toxicological assessments in the ALI exposure system which suggests a complex relationship between the chemical composition of UFP and biological effects in comparison to its size. This can be very critical as the epidemiological and toxicological

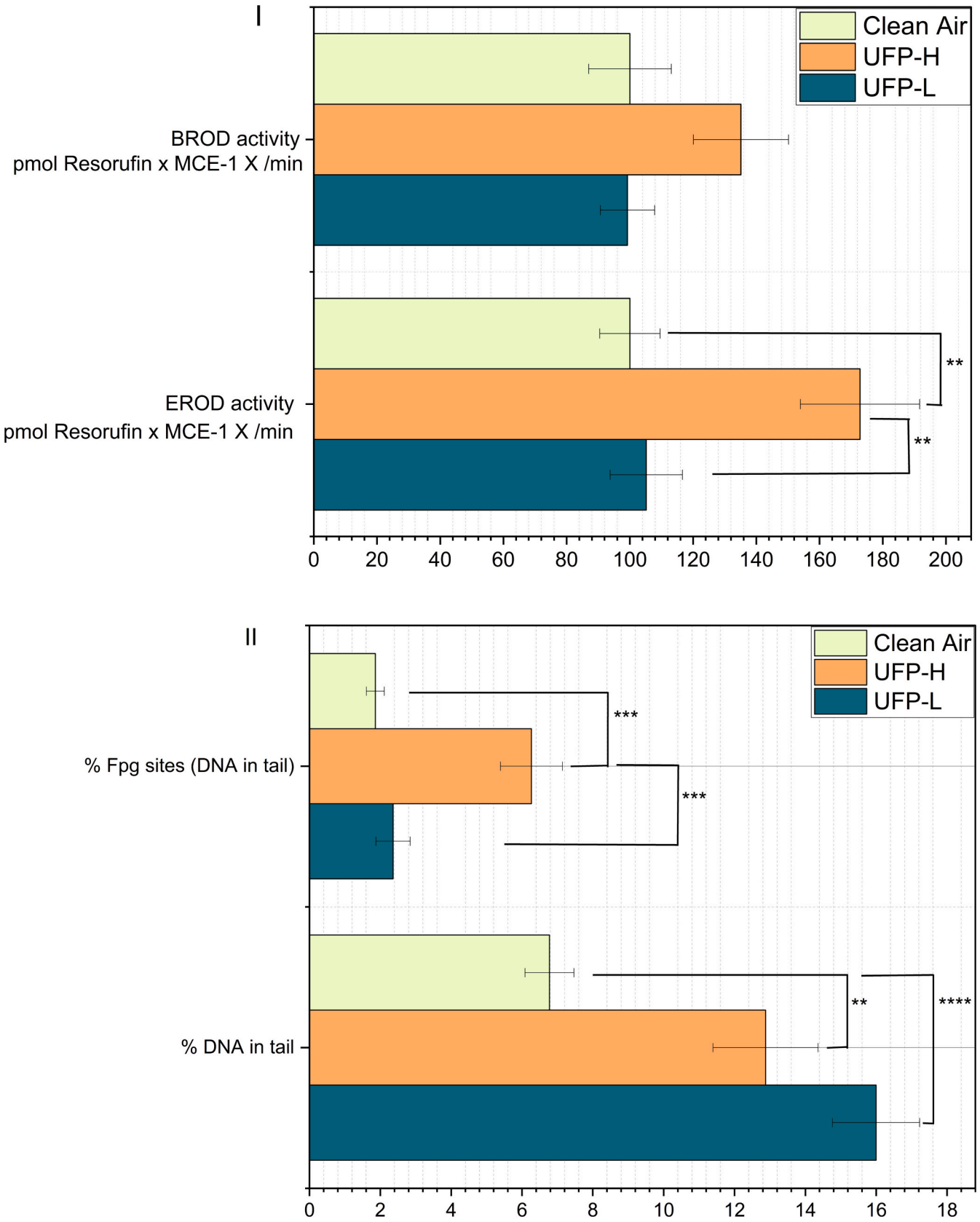

Fig. 6. Cytochrome P450 Activity and DNA Damage. Induction of the resorufin intensity by increased activity of 7-ethoxyresorufin-O-deethylase (EROD) and 7-benzyloxyresorufin-O-debenzylase (BROD) (I) normalized by the metabolic cell equivalent (MCE) following 4 h exposure of A549 cells. Percentage of DNA in tail as well as Fpg sites (% DNA in tail) (II) detected by comet assay following 4 h exposure of A549 cells. UFP-H, UFP with high organic content; UFP-L, UFP with low organic content. Bars represent the average ± s.e.m. (N = 3). Statistically significant results with respect to CA are marked with asterisks (*, $p < 0.05$; **, $p < 0.01$; ***, $p < 0.001$).

literature still lacks evidence-based values for UFP and would provide further knowledge in understanding the limit values of UFP. The high stability and reproducibility of reference UFP production enables repeated ALI exposures, and by applying different dilution ratios, stepwise determination of dose-response investigations is feasible even for direct air-liquid exposures. Future studies will focus on the application of these reference UFP on different cellular models, postexposure responses, transcriptomic and proteomic analyses.

CRediT authorship contribution statement

Anusmita Das: Writing – review & editing, Writing – original draft, Visualization, Validation, Software, Investigation, Formal analysis, Data curation, Conceptualization. **Jana Pantzke:** Writing – review & editing, Writing – original draft, Visualization, Investigation, Data curation, Conceptualization. **Seongho Jeong:** Writing – review & editing, Investigation. **Elena Hartner:** Investigation, Data curation. **Elias J. Zimmermann:** Writing – review & editing, Investigation. **Nadine Gawlitta:** Writing – review & editing, Writing – original draft, Investigation, Data curation. **Svenja Offer:** Writing – review & editing, Investigation, Data curation. **Deeksha Shukla:** Investigation, Data curation. **Anja Huber:** Investigation, Data curation. **Narges Rastak:** Software, Data curation. **Arūnas Meščeriakovas:** Writing – review & editing, Investigation, Data curation. **Natalia P. Ivleva:** Writing – review & editing, Writing – original draft, Investigation, Data curation. **Evelyn Kuhn:** Investigation, Data curation. **Stephanie Binder:** Investigation, Data curation. **Thomas Gröger:** Writing – review & editing, Supervision. **Sebastian Oeder:** Writing – review & editing, Supervision, Investigation, Funding acquisition. **Mathilde Delaval:** Writing – review & editing, Investigation. **Hendryk Czech:** Writing – review & editing, Supervision. **Olli Sippula:** Writing – review & editing, Resources. **Jürgen Schnelle-Kreis:** Writing – review & editing, Writing – original draft, Supervision, Project administration. **Sebastiano Di Bucchianico:** Writing – review & editing, Writing – original draft, Supervision, Resources, Project administration, Investigation, Funding acquisition, Data curation, Conceptualization. **Martin Sklorz:** Writing – review & editing, Writing – original draft, Supervision, Project administration, Methodology, Investigation, Data curation, Conceptualization. **Ralf Zimmermann:** Writing – review & editing, Supervision, Resources, Project administration, Funding acquisition, Conceptualization.

Declaration of competing interest

The authors declare that they have no known competing financial interests or personal relationships that could have appeared to influence the work reported in this paper.

Data availability

Data will be made available on request.

Acknowledgments

Bayerischer Projektverbund Ultrafeine Partikel (BAY UFP)). This research was also supported by the project ULTRHAS – ULtrafine particles from TRansportation – Health Assessment of Sources, a project funded under the EU's Research and Innovation programme Horizon 2020, Grant Agreement No. 955390. H.C. acknowledges funding from the Helmholtz International Laboratory aeroHEALTH (Interlabs-0005).

Appendix A. Supplementary data

Supplementary data to this article can be found online at https://doi.org/10.1016/j.scitotenv.2024.175727.

References

Andersen, M.H.G., Saber, A.T., Clausen, P.A., Pedersen, J.E., Løhr, M., Kermanizadeh, A., Loft, S., Ebbehøj, N., Hansen, Å.M., Pedersen, P.B., Koponen, I.K., Nørskov, E.-C., Møller, P., Vogel, U., 2018. Association between polycyclic aromatic hydrocarbon exposure and peripheral blood mononuclear cell DNA damage in human volunteers during fire extinction exercises. Mutagenesis 33, 105–115. https://doi.org/10.1093/mutage/gex021.

Andreau, K., Leroux, M., Bouharrour, A., 2012. Health and cellular impacts of AirPollutants: from Cytoprotection to cytotoxicity. Biochem. Res. Int. 2012, 493894 https://doi.org/10.1155/2012/493894.

Binder, S., Rastak, N., Karg, E., Huber, A., Kuhn, E., Dragan, G.C., Monsé, C.,Breuer, D., Di Bucchianico, S., Delaval, M.N., Oeder, S., Sklorz, M., Zimmermann, R., 2022. Construction of an In vitro air–liquid interface exposure system to assess the toxicological impact of gas and particle phase of semi-volatile organic compounds. Toxics 10. doi:https://doi.org/10.3390/toxics10120730.

Bladt, H., Ivleva, N.P., Niessner, R., 2014. Internally mixed multicomponent soot:Impact of different salts on soot structure and thermo-chemical properties. J. Aerosol Sci. 70, 26–35. doi:https://doi.org/10.1016/j.jaerosci.2013.11.007.

Bonetta, Sa, Gianotti, V., Bonetta, Si, Gosetti, F., Oddone, M., Gennaro, M.C., Carraro, E., 2009. DNA damage in A549 cells exposed to different extracts of PM2.5 from industrial, urban and highway sites. Chemosphere 77, 1030–1034. https://doi.org/10.1016/j.chemosphere.2009.07.076.

Borgie, M., Dagher, Z., Ledoux, F., Verdin, A., Cazier, F., Martin, P., Hachimi, A., Shirali, P., Greige-Gerges, H., Courcot, D., 2015. Comparison between ultrafine and fine particulate matter collected in Lebanon: chemical characterization, in vitro cytotoxic effects and metabolizing enzymes gene expression in human bronchial epithelial cells. Environ. Pollut. 205, 250–260. https://doi.org/10.1016/j.envpol.2015.05.027.

Cao, X., Padoan, S., Binder, S., Bauer, S., Orasche, J., Rus, C.-M., Mudan, A., Huber, A., Kuhn, E., Oeder, S., Lintelmann, J., Adam, T., Di Bucchianico, S., Zimmermann, R., 2022. A comparative study of persistent DNA oxidation and chromosomal instability induced in vitro by oxidizers and reference airborne particles. Mutat. Res. Toxicol. Environ. Mutagen. 874–875, 503446 https://doi.org/10.1016/j.mrgentox.2022.503446.

Cuesta, A., Dhamelincourt, P., Laureyns, J., Martínez-Alonso, A., Tascón, J.M.D., 1994. Raman microprobe studies on carbon materials. Carbon 32, 1523–1532. https://doi.org/10.1016/0008-6223(94)90148-1.

Di Bucchianico, S., Cappellini, F., Le Bihanic, F., Zhang, Y., Dreij, K., Karlsson, H.L., 2017. Genotoxicity of TiO2 nanoparticles assessed by mini-gel comet assay and micronucleus scoring with flow cytometry. Mutagenesis 32, 127–137. https://doi.org/10.1093/mutage/gew030.

Diabaté, S., Mülhopt, S., Paur, H.-R., Krug, H.F., 2008. The response of a co-culture lung model to fine and ultrafine particles of incinerator Fly ash at the air–liquid Interface. Altern. Lab. Anim 36, 285–298. https://doi.org/10.1177/026119290803600306.

Drinovec, L., Močnik, G., Zotter, P., Prévôt, A.S.H., Ruckstuhl, C., Coz, E., Rupakheti, M., Sciare, J., Müller, T., Wiedensohler, A., Hansen, A.D.A., 2015. The "dual-spot" Aethalometer: an improved measurement of aerosol black carbon with real-time loading compensation. Atmospheric Meas. Tech. 8, 1965–1979. https://doi.org/10.5194/amt-8-1965-2015.

Ess, M.N., Vasilatou, K., 2019. Characterization of a new miniCAST with diffusion flame and premixed flame options: generation of particles with high EC content in the size range 30 nm to 200 nm. Aerosol Sci. Technol. 53, 29–44. https://doi.org/10.1080/02786826.2018.1536818.

Ess, M.N., Ferry, D., Kireeva, E.D., Niessner, R., Ouf, F.-X., Ivleva, N.P., 2016. In situ Raman microspectroscopic analysis of soot samples with different organic carbon content: structural changes during heating. Carbon 105, 572–585. https://doi.org/10.1016/j.carbon.2016.04.056.

Ess, M.N., Bertò, M., Keller, A., Gysel-Beer, M., Vasilatou, K., 2021. Coated soot particles with tunable, well-controlled properties generated in the laboratory with a miniCAST BC and a micro smog chamber. J. Aerosol Sci. 157, 105820 https://doi.org/10.1016/j.jaerosci.2021.105820.

Ferrari, A.C., Robertson, J., 2000. Interpretation of Raman spectra of disordered and amorphous carbon. Phys. Rev. B 61, 14095–14107. https://doi.org/10.1103/PhysRevB.61.14095.

Gawlitta, N., Orasche, J., Geldenhuys, G.-L., Jakobi, G., Wattrus, M., Jennerwein, M., Michalke, B., Gröger, T., Forbes, P., Zimmermann, R., 2023. A study on the chemical profile and the derived health effects of heavy-duty machinery aerosol with a focus on the impact of alternative fuels. Air Qual. Atmos. Health 16, 535–551. https://doi.org/10.1007/s11869-022-01287-9.

Genies, C., Maître, A., Lefèbvre, E., Jullien, A., Chopard-Lallier, M., Douki, T., 2013. The extreme variety of genotoxic response to benzo[a]pyrene in three different human cell lines from three different organs. PLoS One 8, e78356. https://doi.org/10.1371/journal.pone.0078356.

Hakkarainen, H., Järvinen, A., Lepistö, T., Salo, L., Kuittinen, N., Laakkonen, E., Yang, M., Martikainen, M.-V., Saarikoski, S., Aurela, M., Barreira, L., Teinilä, K., Ihalainen, M., Aakko-Saksa, P., Timonen, H., Rönkkö, T., Jalava, P., 2023. Toxicity of exhaust emissions from high aromatic and non-aromatic diesel fuels using in vitro ALI exposure system. Sci. Total Environ. 890, 164215 https://doi.org/10.1016/j.scitotenv.2023.164215.

Hammond, J., Maher, B.A., Gonet, T., Bautista, F., Allsop, D., 2022. Oxidative stress, cytotoxic and inflammatory effects of urban ultrafine road-deposited dust from the UK and Mexico in human epithelial lung (Calu-3) cells. Antioxidants 11. https://doi.org/10.3390/antiox11091814.

Han, D., Chen, R., Kan, H., Xu, Y., 2023. The bio-distribution, clearance pathways, and toxicity mechanisms of ambient ultrafine particles. Eco-Environ. Health 2, 95–106. https://doi.org/10.1016/j.eehl.2023.06.001.

Hatzis, C., Godleski, J.J., González-Flecha, B., Wolfson, J.M., Koutrakis, P., 2006. Ambient particulate matter exhibits direct inhibitory effects on oxidative stress enzymes. Environ. Sci. Technol. 40, 2805–2811. https://doi.org/10.1021/es0518732.

He, R.-W., Gerlofs-Nijland, M.E., Boere, J., Fokkens, P., Leseman, D., Janssen, N.A.H., Cassee, F.R., 2020. Comparative toxicity of ultrafine particles around a major airport in human bronchial epithelial (Calu-3) cell model at the air–liquid interface. Toxicol. in Vitro 68, 104950. https://doi.org/10.1016/j.tiv.2020.104950.

He, R.-W., Houtzager, M.M.G., Jongeneel, W.P., Westerink, R.H.S., Cassee, F.R., 2021. In vitro hazard characterization of simulated aircraft cabin bleed-air contamination in lung models using an air-liquid interface (ALI) exposure system. Environ. Int. 156, 106718 https://doi.org/10.1016/j.envint.2021.106718.

Heinrich, P., Diehl, U., Förster, F., Braunbeck, T., 2014. Improving the in vitro ethoxyresorufin-O-deethylase (EROD) assay with RTL-W1 by metabolic normalization and use of β-naphthoflavone as the reference substance. Comp. Biochem. Physiol. Part C Toxicol. Pharmacol. 164, 27–34. https://doi.org/10.1016/j.cbpc.2014.04.005.

Herzog, K., IJlst, L., van Cruchten, A.G., van Roermund, C.W.T., Kulik, W., Wanders, R.J. A., Waterham, H.R., 2019. An UPLC-MS/MS assay to measure glutathione as marker for oxidative stress in cultured cells. Metabolites 9. https://doi.org/10.3390/metabo9030045.

Hofman, J., Staelens, J., Cordell, R., Stroobants, C., Zikova, N., Hama, S.M.L., Wyche, K. P., Kos, G.P.A., Van Der Zee, S., Smallbone, K.L., Weijers, E.P., Monks, P.S., Roekens, E., 2016. Ultrafine particles in four European urban environments: results from a new continuous long-term monitoring network. Atmos. Environ. 136, 68–81. https://doi.org/10.1016/j.atmosenv.2016.04.010.

Hussar, E., Richards, S., Lin, Z.-Q., Dixon, R.P., Johnson, K.A., 2012. Human health risk assessment of 16 priority polycyclic aromatic hydrocarbons in soils of Chattanooga, Tennessee, USA. Water Air Soil Pollut. 223, 5535–5548. https://doi.org/10.1007/s11270-012-1265-7.

Jing, L., 1999. Standard combustion aerosol generator (SCAG) for calibration purposes. In: Presented at the 3rd ETH Workshop "Nanoparticle Measurement," ETH Hönggerberg Zürich.

Jonsdottir, H.R., Delaval, M., Leni, Z., Keller, A., Brem, B.T., Siegerist, F., Schönenberger, D., Durdina, L., Elser, M., Burtscher, H., Liati, A., Geiser, M., 2019. Non-volatile particle emissions from aircraft turbine engines at ground-idle induce oxidative stress in bronchial cells. Commun. Biol. 2, 90. https://doi.org/10.1038/s42003-019-0332-7.

Juarez-Facio, A.T., Castilla, C., Corbière, C., Lavanant, H., Afonso, C., Morin, C., Merlet-Machour, N., Chevalier, L., Vaugeois, J.-M., Yon, J., Monteil, C., 2022. Development of a standardized in vitro approach to evaluate microphysical, chemical, and toxicological properties of combustion-derived fine and ultrafine particles. J. Environ. Sci. 113, 104–117. https://doi.org/10.1016/j.jes.2021.06.001.

Jung, K.H., Yan, B., Chillrud, S.N., Perera, F.P., Whyatt, R., Camann, D., Kinney, P.L., Miller, R.L., 2010. Assessment of benzo(a)pyrene-equivalent carcinogenicity and mutagenicity of residential indoor versus outdoor polycyclic aromatic hydrocarbons exposing young children in new York City. Int. J. Environ. Res. Public Health 7, 1889–1900. https://doi.org/10.3390/ijerph7051889.

Karg, E.W., Ferron, G.A., Bauer, S., Di Bucchianico, S., Zimmermann, R., 2020. Is the particle deposition in a cell exposure facility comparable to the lungs? A computer model approach. Aerosol Sci. Technol. 54, 668–684. https://doi.org/10.1080/02786826.2020.1724868.

Kim, B., Shin, J.H., Kim, H.P., Jo, M.S., Kim, H.S., Lee, J.S., Lee, H.K., Kwon, H.C., Han, S. G., Kang, N., Gulumian, M., Bello, D., Yu, I.J., 2022. On-Site Deployment of an Air-Liquid-Interphase Device to Assess Health Hazard Potency of Airborne Workplace Contaminants: The Case of 3-D Printers. Front, Toxicol, p. 4.

Leikauf, G.D., Kim, S.-H., Jang, A.-S., 2020. Mechanisms of ultrafine particle-induced respiratory health effects. Exp. Mol. Med. 52, 329–337. https://doi.org/10.1038/s12276-020-0394-0.

León-Mejía, G., Silva, L.F.O., Civeira, M.S., Oliveira, M.L.S., Machado, M., Villela, I.V., Hartmann, A., Premoli, S., Corrêa, D.S., Da Silva, J., Henriques, J.A.P., 2016. Cytotoxicity and genotoxicity induced by coal and coal fly ash particles samples in V79 cells. Environ. Sci. Pollut. Res. 23, 24019–24031. https://doi.org/10.1007/s11356-016-7623-z.

Liu, C., Chung, C.E., Yin, Y., Schnaiter, M., 2018. The absorption Ångström exponent of black carbon: from numerical aspects. Atmos. Chem. Phys. 18, 6259–6273. https://doi.org/10.5194/acp-18-6259-2018.

Liu, X., Deming, B., Pagonis, D., Day, D.A., Palm, B.B., Talukdar, R., Roberts, J.M., Veres, P.R., Krechmer, J.E., Thornton, J.A., de Gouw, J.A., Ziemann, P.J., Jimenez, J. L., 2019. Effects of gas–wall interactions on measurements of semivolatile compounds and small polar molecules. Atmospheric Meas. Tech. 12, 3137–3149. https://doi.org/10.5194/amt-12-3137-2019.

Lucci, F., Castro, N.D., Rostami, A.A., Oldham, M.J., Hoeng, J., Pithawalla, Y.B., Kuczaj, A.K., 2018. Characterization and modeling of aerosol deposition in Vitrocell® exposure systems - exposure well chamber deposition efficiency. J. Aerosol Sci. 123, 141–160. https://doi.org/10.1016/j.jaerosci.2018.06.015.

Malmborg, V.B., Eriksson, A.C., Török, S., Zhang, Y., Kling, K., Martinsson, J., Fortner, E. C., Gren, L., Kook, S., Onasch, T.B., Bengtsson, P.-E., Pagels, J., 2019. Relating aerosol mass spectra to composition and nanostructure of soot particles. Carbon 142, 535–546. https://doi.org/10.1016/j.carbon.2018.10.072.

Marhaba, I., Ferry, D., Laffon, C., Regier, T.Z., Ouf, F.-X., Parent, P., 2019. Aircraft and MiniCAST soot at the nanoscale. Combust. Flame 204, 278–289. https://doi.org/10.1016/j.combustflame.2019.03.018.

Mason, Y.C., Schoonraad, G.-L., Orasche, J., Bisig, C., Jakobi, G., Zimmermann, R., Forbes, P.B.C., 2020. Comparative sampling of gas phase volatile and semi-volatile organic fuel emissions from a combustion aerosol standard system. Environ. Technol. Innov. 19, 100945 https://doi.org/10.1016/j.eti.2020.100945.

Moallemi, A., Kazemimanesh, M., Corbin, J.C., Thomson, K., Smallwood, G., Olfert, J.S., Lobo, P., 2019. Characterization of black carbon particles generated by a propane-fueled miniature inverted soot generator. J. Aerosol Sci. 135, 46–57. https://doi.org/10.1016/j.jaerosci.2019.05.004.

Moore, R.H., Ziemba, L.D., Dutcher, D., Beyersdorf, A.J., Chan, K., Crumeyrolle, S., Raymond, T.M., Thornhill, K.L., Winstead, E.L., Anderson, B.E., 2014. Mapping the operation of the miniature combustion aerosol standard (Mini-CAST) soot generator. Aerosol Sci. Technol. 48, 467–479. https://doi.org/10.1080/02786826.2014.890694.

Moosmüller, H., Arnott, W.P., Rogers, C.F., Bowen, J.L., Gillies, J.A., Pierson, W.R., Collins, J.F., Durbin, T.D., Norbeck, J.M., 2001. Time-resolved characterization of diesel particulate emissions. 2. Instruments for elemental and organic carbon measurements. Environ. Sci. Technol. 35, 1935–1942. https://doi.org/10.1021/es0015242.

Moreno-Ríos, A.L., Tejeda-Benítez, L.P., Bustillo-Lecompte, C.F., 2022. Sources, characteristics, toxicity, and control of ultrafine particles: an overview. Geosci. Front. 13, 101147 https://doi.org/10.1016/j.gsf.2021.101147.

Mülhopt, S., Dilger, M., Diabaté, S., Schlager, C., Krebs, T., Zimmermann, R., Buters, J., Oeder, S., Wäscher, T., Weiss, C., Paur, H.-R., 2016. Toxicity testing of combustion aerosols at the air–liquid interface with a self-contained and easy-to-use exposure system. J. Aerosol Sci. 96, 38–55. https://doi.org/10.1016/j.jaerosci.2016.02.005.

Ngo, L.D., Duca, D., Carpentier, Y., Noble, J.A., Ikhenazene, R., Vojkovic, M., Irimiea, C., Ortega, I.K., Lefevre, G., Yon, J., Faccinetto, A., Therssen, E., Ziskind, M., Chazallon, B., Pirim, C., Focsa, C., 2020. Chemical discrimination of the particulate and gas phases of miniCAST exhausts using a two-filter collection method. Atmospheric Meas. Tech. 13, 951–967. https://doi.org/10.5194/amt-13-951-2020.

Oeder, S., Kanashova, T., Sippula, O., Sapcariu, S.C., Streibel, T., Arteaga-Salas, J.M., Passig, J., Dilger, M., Paur, H.-R., Schlager, C., Mülhopt, S., Diabaté, S., Weiss, C., Stengel, B., Rabe, R., Harndorf, H., Torvela, T., Jokiniemi, J.K., Hirvonen, M.-R., Schmidt-Weber, C., Traidl-Hoffmann, C., BéruBé, K.A., Wlodarczyk, A.J., Prytherch, Z., Michalke, B., Krebs, T., Prévôt, A.S.H., Kelbg, M., Tiggesbäumker, J., Karg, E., Jakobi, G., Scholtes, S., Schnelle-Kreis, J., Lintelmann, J., Matuschek, G., Sklorz, M., Klingbeil, S., Orasche, J., Richthammer, P., Müller, L., Elsasser, M., Reda, A., Gröger, T., Weggler, B., Schwemer, T., Czech, H., Rüger, C.P., Abbaszade, G., Radischat, C., Hiller, K., Buters, J.T.M., Dittmar, G., Zimmermann, R., 2015. Particulate matter from both heavy fuel oil and diesel fuel shipping emissions show strong biological effects on human lung cells at realistic and comparable in vitro exposure conditions. PLoS One 10, e0126536. https://doi.org/10.1371/journal.pone.0126536.

Offer Svenja, Hartner Elena, Di Bucchianico Sebastiano, Bisig Christoph, Bauer Stefanie, Pantzke Jana, Zimmermann Elias J., Cao Xin, Binder Stefanie, Kuhn Evelyn, Huber Anja, Jeong Seongho, Käfer Uwe, Martens Patrick, Mesceriakovas Arunas, Bendl Jan, Brejcha Ramona, Buchholz Angela, Gat Daniella, Hohaus Thorsten, Rastak Narges, Jakobi Gert, Kalberer Markus, Kanashova Tamara, Hu Yue, Ogris Christoph, Marsico Annalisa, Theis Fabian, Pardo Michal, Gröger Thomas, Oeder Sebastian, Orasche Jürgen, Paul Andreas, Ziehm Till, Zhang Zhi-Hui, Adam Thomas, Sippula Olli, Sklorz Martin, Schnelle-Kreis Jürgen, Czech Hendryk, Kiendler-Scharr Astrid, Rudich Yinon, Zimmermann Ralf, n.d. Effect of atmospheric aging on soot particle toxicity in lung cell models at the air–liquid Interface: differential toxicological impacts of biogenic and anthropogenic secondary organic aerosols (SOAs). Environ. Health Perspect. 130, 027003. doi:https://doi.org/10.1289/EHP9413.

Ohlwein, S., Kappeler, R., Kutlar Joss, M., Künzli, N., Hoffmann, B., 2019. Health effects of ultrafine particles: a systematic literature review update of epidemiological evidence. Int. J. Public Health 64, 547–559. https://doi.org/10.1007/s00038-019-01202-7.

Orasche, J., Schnelle-Kreis, J., Abbaszade, G., Zimmermann, R., 2011. Technical note: in-situ derivatization thermal desorption GC-TOFMS for direct analysis of particle-bound non-polar and polar organic species. Atmos. Chem. Phys. 11, 8977–8993. https://doi.org/10.5194/acp-11-8977-2011.

Øvrevik, J., Refsnes, M., Låg, M., Holme, J.A., Schwarze, P.E., 2015. Activation of Proinflammatory responses in cells of the airway mucosa by particulate matter: oxidant- and non-oxidant-mediated triggering mechanisms. Biomolecules 5, 1399–1440. https://doi.org/10.3390/biom5031399.

Pardo, M., Offer, S., Hartner, E., Di Bucchianico, S., Bisig, C., Bauer, S., Pantzke, J., Zimmermann, E.J., Cao, X., Binder, S., Kuhn, E., Huber, A., Jeong, S., Käfer, U., Schneider, E., Mesceriakovas, A., Bendl, J., Brejcha, R., Buchholz, A., Gat, D., Hohaus, T., Rastak, N., Karg, E., Jakobi, G., Kalberer, M., Kanashova, T., Hu, Y., Ogris, C., Marsico, A., Theis, F., Shalit, T., Gröger, T., Rüger, C.P., Oeder, S., Orasche, J., Paul, A., Ziehm, T., Zhang, Z.-H., Adam, T., Sippula, O., Sklorz, M., Schnelle-Kreis, J., Czech, H., Kiendler-Scharr, A., Zimmermann, R., Rudich, Y., 2022. Exposure to naphthalene and β-pinene-derived secondary organic aerosol induced divergent changes in transcript levels of BEAS-2B cells. Environ. Int. 166, 107366 https://doi.org/10.1016/j.envint.2022.107366.

Pardo, M., Czech, H., Offer, S., Sklorz, M., Di Bucchianico, S., Hartner, E., Pantzke, J., Kuhn, E., Paul, A., Ziehm, T., Zhang, Z.-H., Jakobi, G., Bauer, S., Huber, A., Zimmermann, E.J., Rastak, N., Binder, S., Brejcha, R., Schneider, E., Orasche, J., Rüger, C.P., Gröger, T., Oeder, S., Schnelle-Kreis, J., Hohaus, T., Kalberer, M., Sippula, O., Kiendler-Scharr, A., Zimmermann, R., Rudich, Y., 2023. Atmospheric aging increases the cytotoxicity of bare soot particles in BEAS-2B lung cells. Aerosol Sci. Technol. 57, 367–383. https://doi.org/10.1080/02786826.2023.2178878.

Paur, H.-R., Cassee, F.R., Teeguarden, J., Fissan, H., Diabate, S., Aufderheide, M., Kreyling, W.G., Hänninen, O., Kasper, G., Riediker, M., Rothen-Rutishauser, B.,

Schmid, O., 2011. In-vitro cell exposure studies for the assessment of nanoparticle toxicity in the lung—a dialog between aerosol science and biology. J. Aerosol Sci. 42, 668–692. https://doi.org/10.1016/j.jaerosci.2011.06.005.
Perron, N., Sandradewi, J., Alfarra, M.R., Lienemann, P., Gehrig, R., Kasper-Giebl, A., Lanz, V.A., Szidat, S., Ruff, M., Fahrni, S., Wacker, L., Baltensperger, U., Prévôt, A.S. H., 2010. Composition and sources of particulate matter in an industrialised alpine valley. Atmospheric Chem. Phys. Discuss. 10, 9391–9430. https://doi.org/10.5194/acpd-10-9391-2010.
Petzold, A., Ogren, J.A., Fiebig, M., Laj, P., Li, S.-M., Baltensperger, U., Holzer-Popp, T., Kinne, S., Pappalardo, G., Sugimoto, N., Wehrli, C., Wiedensohler, A., Zhang, X.-Y., 2013. Recommendations for reporting "black carbon" measurements. Atmos. Chem. Phys. 13, 8365–8379. https://doi.org/10.5194/acp-13-8365-2013.
Rahman, I., MacNee, W., 2000. Oxidative stress and regulation of glutathione in lung inflammation. Eur. Respir. J. 16, 534. https://doi.org/10.1034/j.1399-3003.2000.016003534.x.
Raiolo, A., Stockinger, C., Tuttlies, U., Ivleva, N.P., Shadloo, M.S., Nieken, U., 2024. Effect of nanostructure and BET surface area on the oxygen reactivity of soot filter cakes. Carbon 227, 119251. https://doi.org/10.1016/j.carbon.2024.119251.
Romano, M., González Gómez, M.A., Santonicola, P., Aloi, N., Offer, S., Pantzke, J., Raccosta, S., Longo, V., Surpi, A., Alacqua, S., Zampi, G., Dediu, V.A., Michalke, B., Zimmerman, R., Manno, M., Piñeiro, Y., Colombo, P., Di Schiavi, E., Rivas, J., Bergese, P., Di Bucchianico, S., 2023. Synthesis and characterization of a biocompatible Nanoplatform based on silica-embedded SPIONs functionalized with Polydopamine. ACS Biomater Sci. Eng. 9, 303–317. https://doi.org/10.1021/acsbiomaterials.2c00946.
Romshoo, B., Pöhlker, M., Wiedensohler, A., Pfeifer, S., Saturno, J., Nowak, A., Ciupek, K., Quincey, P., Vasilatou, K., Ess, M.N., Gini, M., Eleftheriadis, K., Robins, C., Gaie-Levrel, F., Müller, T., 2022. Importance of size representation and morphology in modelling optical properties of black carbon: comparison between laboratory measurements and model simulations. Atmospheric Meas. Tech. 15, 6965–6989. https://doi.org/10.5194/amt-15-6965-2022.
Roper, C., Simonich, S.L.M., Tanguay, R.L., 2018. Development of a high-throughput in vivo screening platform for particulate matter exposures. Environ. Pollut. 235, 993–1005. https://doi.org/10.1016/j.envpol.2018.01.025.
Roper, C., Delgado, L.S., Barrett, D., Massey Simonich, S.L., Tanguay, R.L., 2019. PM2.5 filter extraction methods: implications for chemical and toxicological analyses. Environ. Sci. Technol. 53, 434–442. https://doi.org/10.1021/acs.est.8b04308.
Salinas, M.E., Gutiérrez, D.A., Varela-Ramírez, A., Garza, K.M., 2020. Continuous exposure to low doses of ultrafine black carbon reduces the vitality of immortalized lung-derived cells and activates senescence. J. Toxicol. 2020, 5702024. https://doi.org/10.1155/2020/5702024.
Samburova, V., Connolly, J., Gyawali, M., Yatavelli, R.L.N., Watts, A.C., Chakrabarty, R. K., Zielinska, B., Moosmüller, H., Khlystov, A., 2016. Polycyclic aromatic hydrocarbons in biomass-burning emissions and their contribution to light absorption and aerosol toxicity. Sci. Total Environ. 568, 391–401. https://doi.org/10.1016/j.scitotenv.2016.06.026.
Schneider, E., Giocastro, B., Rüger, C.P., Adam, T.W., Zimmermann, R., 2022. Detection of polycyclic aromatic hydrocarbons in high organic carbon ultrafine particle extracts by electrospray ionization ultrahigh-resolution mass spectrometry. J. Am. Soc. Mass Spectrom. 33, 2019–2023. https://doi.org/10.1021/jasms.2c00163.
Schnelle-Kreis, J., Welthagen, W., Sklorz, M., Zimmermann, R., 2005. Application of direct thermal desorption gas chromatography and comprehensive two-dimensional gas chromatography coupled to time of flight mass spectrometry for analysis of organic compounds in ambient aerosol particles. J. Sep. Sci. 28, 1648–1657. https://doi.org/10.1002/jssc.200500120.
Schraufnagel, D.E., 2020. The health effects of ultrafine particles. Exp. Mol. Med. 52, 311–317. https://doi.org/10.1038/s12276-020-0403-3.
Schwarz, M., Schneider, A., Cyrys, J., Bastian, S., Breitner, S., Peters, A., 2023. Impact of ambient ultrafine particles on cause-specific mortality in three German cities. Am. J. Respir. Crit. Care Med. 207, 1334–1344. https://doi.org/10.1164/rccm.202209-1837OC.
Schwarze, P.E., Øvrevik, J., Hetland, R.B., Becher, R., Cassee, F.R., Låg, M., Løvik, M., Dybing, E., Refsnes, M., 2007. Importance of size and composition of particles for effects on cells in vitro. Inhal. Toxicol. 19, 17–22. https://doi.org/10.1080/08958370701490445.
Segura, S., Estellés, V., Titos, G., Lyamani, H., Utrillas, M.P., Zotter, P., Prévôt, A.S.H., Močnik, G., Alados-Arboledas, L., Martínez-Lozano, J.A., 2014. Determination and analysis of in situ spectral aerosol optical properties by a multi-instrumental approach. Atmospheric Meas. Tech. 7, 2373–2387. https://doi.org/10.5194/amt-7-2373-2014.
Shimada, T., Fujii-Kuriyama, Y., 2004. Metabolic activation of polycyclic aromatic hydrocarbons to carcinogens by cytochromes P450 1A1 and1B1. Cancer Sci. 95, 1–6. https://doi.org/10.1111/j.1349-7006.2004.tb03162.x.
Singh, A.V., Romeo, A., Scott, K., Wagener, S., Leibrock, L., Laux, P., Luch, A., Kerkar, P., Balakrishnan, S., Dakua, S.P., Park, B.-W., 2021. Emerging Technologies for in Vitro Inhalation Toxicology. Adv. Healthc. Mater. 10, 2100633. https://doi.org/10.1002/adhm.202100633.
Sun, X., Berger, R.S., Heinrich, P., Marchiq, I., Pouyssegur, J., Renner, K., Oefner, P.J., Dettmer, K., 2020. Optimized protocol for the in situ derivatization of glutathione with N-Ethylmaleimide in cultured cells and the simultaneous determination of glutathione/glutathione disulfide ratio by HPLC-UV-QTOF-MS. Metabolites 10. https://doi.org/10.3390/metabo10070292.
Swanson, J., Kittelson, D., 2010. Evaluation of thermal denuder and catalytic stripper methods for solid particle measurements. J. Aerosol Sci. 41, 1113–1122. https://doi.org/10.1016/j.jaerosci.2010.09.003.
Thorne, D., Adamson, J., 2013. A review of in vitro cigarette smoke exposure systems. Exp. Toxicol. Pathol. 65, 1183–1193. https://doi.org/10.1016/j.etp.2013.06.001.
Tsikas, D., 2017. Assessment of lipid peroxidation by measuring malondialdehyde (MDA) and relatives in biological samples: analytical and biological challenges. Lipid Methodol. 524, 13–30. https://doi.org/10.1016/j.ab.2016.10.021.
Tuinstra, F., Koenig, J.L., 1970. Raman Spectrum of graphite. J. Chem. Phys. 53, 1126–1130. https://doi.org/10.1063/1.1674108.
Upadhyay, S., Palmberg, L., 2018. Air-liquid Interface: relevant in vitro models for investigating air pollutant-induced pulmonary toxicity. Toxicol. Sci. 164, 21–30. https://doi.org/10.1093/toxsci/kfy053.
Vallabani, N.V.S., Gruzieva, O., Elihn, K., Juárez-Facio, A.T., Steimer, S.S., Kuhn, J., Silvergren, S., Portugal, J., Piña, B., Olofsson, U., Johansson, C., Karlsson, H.L., 2023. Toxicity and health effects of ultrafine particles: towards an understanding of the relative impacts of different transport modes. Environ. Res. 231, 116186 https://doi.org/10.1016/j.envres.2023.116186.
Vander Wal, R.L., Tomasek, A.J., 2004. Soot nanostructure: dependence upon synthesis conditions. Combust. Flame 136, 129–140. https://doi.org/10.1016/j.combustflame.2003.09.008.
Vander Wal, R.L., Yezerets, A., Currier, N.W., Kim, D.H., Wang, C.M., 2007. HRTEM study of diesel soot collected from diesel particulate filters. Carbon 45, 70–77. https://doi.org/10.1016/j.carbon.2006.08.005.
Virkkula, A., 2021. Modeled source apportionment of black carbon particles coated with a light-scattering shell. Atmospheric Meas. Tech. 14, 3707–3719. https://doi.org/10.5194/amt-14-3707-2021.
WHO global air quality guidelines: particulate matter (PM2.5 and PM10), ozone, nitrogen dioxide, sulfur dioxide and carbon monoxide, 2021.
Wohak, L.E., Krais, A.M., Kucab, J.E., Stertmann, J., Øvrebø, S., Seidel, A., Phillips, D.H., Arlt, V.M., 2016. Carcinogenic polycyclic aromatic hydrocarbons induce CYP1A1 in human cells via a p53-dependent mechanism. Arch. Toxicol. 90, 291–304. https://doi.org/10.1007/s00204-014-1409-1.
Zotter, P., Herich, H., Gysel, M., El-Haddad, I., Zhang, Y., Močnik, G., Hüglin, C., Baltensperger, U., Szidat, S., Prévôt, A.S.H., 2017. Evaluation of the absorption Ångström exponents for traffic and wood burning in the Aethalometer-based source apportionment using radiocarbon measurements of ambient aerosol. Atmos. Chem. Phys. 17, 4229–4249. https://doi.org/10.5194/acp-17-4229-2017.